Article

Neuron

How mRNA Localization and Protein Synthesis Sites Influence Dendritic Protein Distribution and Dynamics

Graphical Abstract

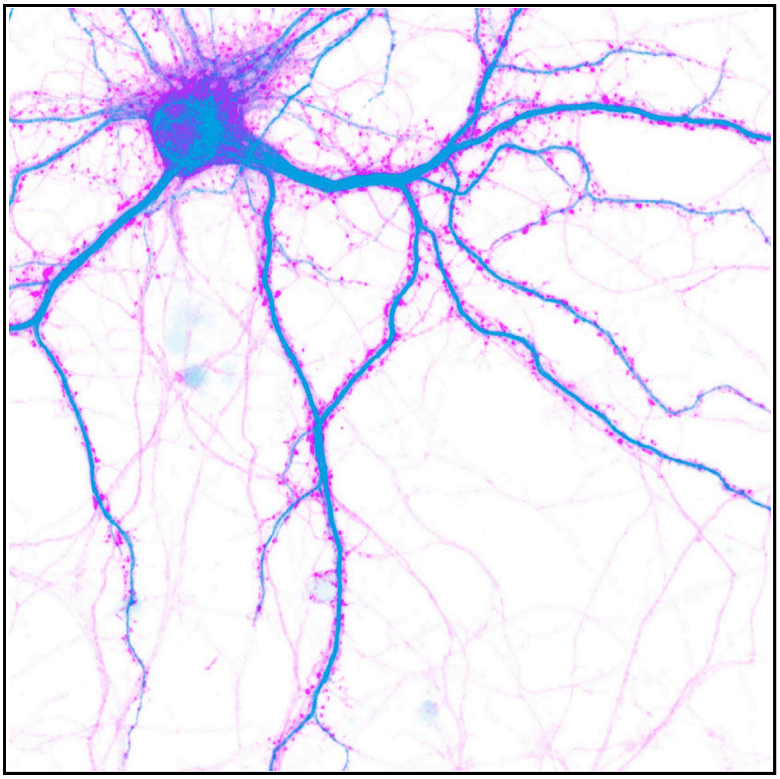

Highlights

- More than half of CamKIIα proteins are synthesized in dendrites
- mRNA transport velocity and lifetime have a large impact on protein localization
- Dendritic protein synthesis largely contributes to populating distal dendrites
- Translational bursts can alter protein counts for hours over hundreds of micrometers

Authors

Yombe Fonkeu, Nataliya Kraynyukova, Anne-Sophie Hafner, Lisa Kochen, Fabio Sartori, Erin M. Schuman, Tatjana Tchumatchenko

Correspondence

tatjana.tchumatchenko@brain.mpg.de

In Brief

A steady protein supply is critical to synaptic function. Here, Fonkeu et al. present a theoretical framework, validated by experimental data, that details how local and dendritic mRNAs shape dendritic protein dynamics across short and long timescales.

Fonkeu et al., 2019, Neuron *103*, 1109–1122
September 25, 2019 © 2019 Elsevier Inc.
https://doi.org/10.1016/j.neuron.2019.06.022

Neuron
Article

How mRNA Localization and Protein Synthesis Sites Influence Dendritic Protein Distribution and Dynamics

Yombe Fonkeu,[1,3,4] Nataliya Kraynyukova,[1,4] Anne-Sophie Hafner,[2,4] Lisa Kochen,[2] Fabio Sartori,[1] Erin M. Schuman,[2] and Tatjana Tchumatchenko[1,5,*]
[1]Max Planck Institute for Brain Research, Theory of Neural Dynamics Group, Frankfurt am Main, Germany
[2]Max Planck Institute for Brain Research, Department of Synaptic Plasticity, Frankfurt am Main, Germany
[3]Emory University School of Medicine, Atlanta, GA, USA
[4]These authors contributed equally
[5]Lead Contact
*Correspondence: tatjana.tchumatchenko@brain.mpg.de
https://doi.org/10.1016/j.neuron.2019.06.022

SUMMARY

Proteins drive the function of neuronal synapses. The synapses are distributed throughout the dendritic arbor, often hundreds of micrometers away from the soma. It is still unclear how somatic and dendritic sources of proteins shape protein distribution and respectively contribute to local protein changes during synaptic plasticity. Here, we present a unique computational framework describing for a given protein species the dendritic distribution of the mRNA and the corresponding protein in a dendrite. Using CaMKIIα as a test case, our model reveals the key role active transport plays in the maintenance of dendritic mRNA and protein levels and predicts the short and long timescales of protein dynamics. Our model reveals the fundamental role of mRNA localization and dendritic mRNA translation in synaptic maintenance and plasticity in distal compartments. We developed a web application for neuroscientists to explore the dynamics of the mRNA or protein of interest.

INTRODUCTION

Neurons, like all other cells, require proteins to function. A single neuron expresses ∼12,000 protein species, and each of these proteins is produced from its corresponding mRNA in the soma or in the neurites. Because the dendrites can extend hundreds of micrometers from the cell body, understanding how changes in synaptic protein composition are resolved in space and time is particularly challenging. Recent studies have revealed that most proteins, including synaptic proteins, have half-lives that range between 5 and 7 days (Cohen et al., 2013; Dörrbaum et al., 2018). Thus, to maintain synaptic function, neurons have to constantly produce, target, and degrade synaptic proteins. During synaptic plasticity, long-lasting changes in the protein composition of individual synapses result in the modulation of synaptic efficacies. Remarkably, despite the highly unstable nature of its main components, our brain is capable of storing memories over decades.

Growing experimental evidence indicates that mRNAs are abundant in dendrites (Cajigas et al., 2012; Tushev et al., 2018), and an extensive body of literature shows that local translation plays an important role in many forms of developmental and synaptic plasticity (reviewed in Holt and Schuman, 2013; Glock et al., 2017). Interestingly, preventing the dendritic localization of CaMKIIα mRNA, a major kinase in synaptic plasticity, alters the protein concentration at synapses as well as synaptic and behavioral plasticity (Miller et al., 2002). Producing proteins directly in dendrites rather than in the soma may provide multiple advantages: (1) limiting cost for transport and storage, (2) increasing protein yield by limiting degradation en route, and (3) allowing rapid "on demand" production of proteins for quick incorporation into local complexes (Hanus and Schuman, 2013).

Theory-based attempts to understand long-range dendritic protein distributions often assume a central protein source at the cell body and disregard the role of dendritic mRNAs in protein synthesis (Bressloff and Newby, 2013; Bressloff and Earnshaw, 2007; Williams et al., 2016). While this may be a good assumption for some proteins whose mRNAs are confined to the cell body, many neuronal proteins have their mRNA in dendrites. Prior models have also often focused on steady-state protein quantities across large distances that arise from a point source and then diffuse or are actively transported (Bressloff and Newby, 2013). Interestingly, models based on a somatic point source of proteins (Doyle and Kiebler, 2011; Williams et al., 2016) often cannot capture experimental data showing fast and highly accurate responses to activity in distal compartments (e.g., Smith et al., 2005; Sutton and Schuman, 2006). Also, models that account for local protein synthesis rate are often limited to a small dendritic compartment (Czöndör et al., 2012; Ranft et al., 2017; Triesch et al., 2018) and their predictions cannot easily be extended to describe long-range aspects of mRNA and protein dynamics. Recent experiments revealed that both transcription of mRNAs and synthesis of proteins are not constant, as many models assume, but are highly dynamic

© 2019 Elsevier Inc.

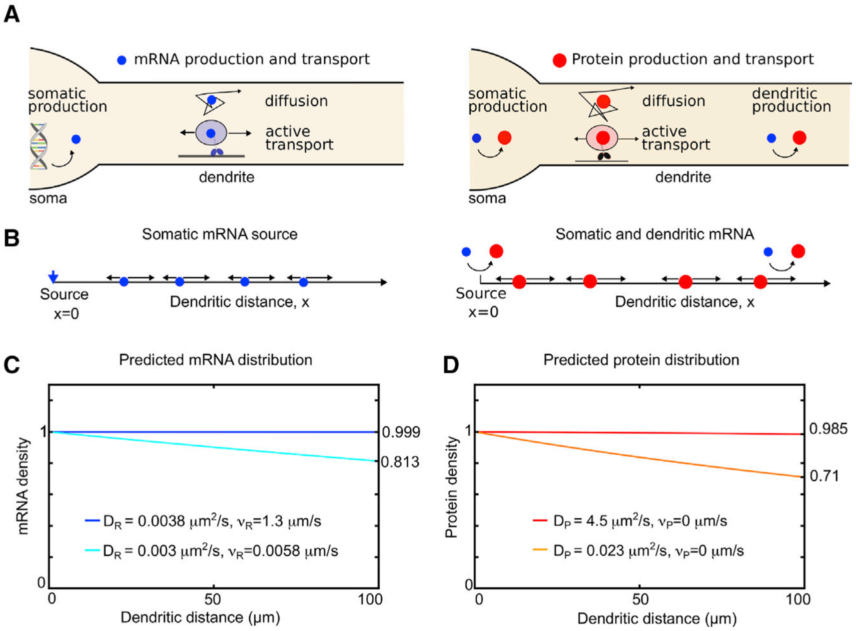

Figure 1. Construction of the Model and Its Predictions

(A) The mRNAs are synthesized in the soma and move into the dendrite either via active motor-mediated transport along microtubules (with an average directed velocity ν_R) or via passive diffusive motion (diffusion coefficient D_R). Proteins are synthesized from somatic or dendritic mRNAs and can either diffuse (diffusion coefficient D_P) or be actively transported along microtubules (average velocity ν_P). Many dendritic proteins (including CamKIIα) only undergo passive diffusion ($\nu_P = 0$), while some selected protein classes (e.g., membranous organelles or macromolecular complexes) can be actively transported along microtubules (Hirokawa and Takemura, 2005) ($\nu_P \neq 0$). Our model accounts for both classes.

(B) A one-dimensional model representation of the mRNA and protein dynamics. The downward blue arrow indicates that the only source of mRNAs is at the $x = 0$ position.

(C and D) We derived a prediction for the spatial distribution of mRNAs (C) and proteins (D) using Equations 2, 4, and 5. Candidate parameters for the diffusion and transport velocity of mRNA and proteins are obtained from the literature (see Table 2), and the ratio of somatic and dendritic mRNAs is inferred from Miller et al. (2002). Color code denotes the upper bound (dark blue and red) and lower bound (light blue and orange) for the respective distributions.

in time and across space, with a dependence on the synaptic activity (Wu et al., 2016; Dieterich et al., 2010). Incorporating these new aspects into a comprehensive and quantitative framework that can account for both local and long-range dynamics is necessary to keep pace with the rapidly expanding experimental toolkit visualizing the dynamics of both dendritic RNAs and proteins *in situ* (Dieterich et al., 2010; Akbalik et al., 2017; Yoon et al., 2016; Buxbaum et al., 2015).

Here, we present a model framework able to capture the spatial profile of mRNA and their corresponding proteins while also accounting for the many experimentally observed properties of protein dynamics on short and long timescales. Our model encompasses various processes involved in the intracellular trafficking of molecules from the soma to the dendrites, including production and degradation, as well as uni- and bi-directional transport. In order to validate the results of our model, we use CaMKIIα experimental data. Crucially, we predict the spatial profile and the timescales of protein response following locally induced changes in translation. We also provide an online web application for our readers to explore the dynamics of their mRNAs and proteins of interest in dendrites (http://www.tchumatchenko.de/Visualisation.html).

RESULTS

Deriving the mRNA and Protein Distributions

Our goal is to understand how the processes of transcription, translation, trafficking, and degradation shape the dendritic distribution of mRNAs and their corresponding proteins. We start by summarizing the spatial and temporal characteristics of these basic biological processes and explain how we incorporate them into our mathematical model (Figure 1A). The mRNAs are produced in the cell nucleus, a process known as transcription, and are rapidly transported into the somatic cytoplasm. Cytoplasmic mRNAs can then move into the dendrites via diffusion (Fusco et al., 2003) or active microtubule-mediated transport (Kanai et al., 2004) (Figures 1A and 1B, left). We assume a source term at $x = 0$, which corresponds to a somatic transcription rate β_R. We describe the basic transport, production, and degradation mechanisms of mRNAs in the dendrites ($x > 0$) using the following one-dimensional dynamical equation:

$$\frac{\partial R(x,t)}{\partial t} = D_R \frac{\partial^2 R(x,t)}{\partial x^2} - \nu_R \frac{\partial R(x,t)}{\partial x} - k_R R(x,t). \qquad \text{(Equation 1)}$$

Here, $R(x,t)$ represents the distribution of mRNAs as a function of space x and time t. The location x denotes the dendritic distance. We consider all mRNAs that were transcribed from $t = 0$ onward. $\partial/\partial t$, $\partial/\partial x$, and $\partial^2/\partial x^2$ denote the derivatives with respect to time and space. Equation 1 describes the mRNA dynamics and includes passive diffusion with a diffusion coefficient D_R, active transport with an average velocity ν_R, and a degradation rate k_R, see Table 1. In STAR Methods, we present a closed-form solution of Equation 1 and show that with time, it converges toward a state where transport, degradation, and production balance out. This state is described by

$$R_{ss}^{\text{den}}(x) = \frac{\beta_R \lambda_R}{k_R} \exp(-\lambda_R x), \qquad \text{(Equation 2)}$$

where $\lambda_R = \left(\sqrt{\nu_R^2 + 4D_R k_R} - \nu_R\right)/(2D_R)$.

Protein synthesis can take place in the soma from somatic mRNAs or in the dendrites from local dendritic mRNAs R_{ss}^{den}

Table 1. Symbol Nomenclature

mRNA		Protein	
D_R	diffusion coefficient for mRNA	D_P	diffusion coefficient for protein
ν_R	transport velocity of mRNA granule	ν_P	transport velocity of protein vesicle
k_R	degradation rate of mRNA	k_P	degradation rate of protein
β_R	transcription rate of mRNA	β_P	translation rate of protein

(Holt and Schuman, 2013; Tushev et al., 2018). Similar to their mRNA counterparts, proteins can also diffuse passively (e.g., Dieterich et al., 2010) or be transported actively along microtubules (Franker and Hoogenraad, 2013) (Figures 1A and 1B, right).

In cells with a low spine density of 1–2 spines/μm, such as pyramidal neurons (Fiala and Harris, 1999), protein diffusion can be described by normal diffusion (Santamaria et al., 2006). We note that for higher spine densities, a case not described here, protein movement in cells can be described by anomalous diffusion (Santamaria et al., 2006; Pfeiffer et al., 2018). We assume a source term at $x = 0$, which corresponds to a somatic protein synthesis rate β_P. Dendritic protein dynamics for $x > 0$ are then described by the following equation:

$$\frac{\partial P(x,t)}{\partial t} = D_P\frac{\partial^2 P(x,t)}{\partial x^2} - \nu_P\frac{\partial P(x,t)}{\partial x} - k_P P(x,t) + \beta_P R_{ss}^{\mathrm{den}}(x). \qquad \text{(Equation 3)}$$

All proteins that are synthesized from $t = 0$ onward contribute to the protein distribution. We include diffusion characterized by the diffusion coefficient D_P, active transport with an average velocity ν_P, a degradation rate k_P, and an average translation rate β_P, see Table 1. The protein dynamics in Equation 3 converge toward the following distribution in which mRNA and protein transport, production, and degradation processes balance out:

$$P_{ss}^{\mathrm{den}}(x) = \frac{\beta_P\beta_R\lambda_R}{k_R\left(D_P\lambda_R^2 + \nu_P\lambda_R - k_P\right)}\left(-e^{-\lambda_R x} + \frac{D_P\lambda_P\lambda_R + \nu_P\lambda_P}{k_P}e^{-\lambda_P x}\right). \qquad \text{(Equation 4)}$$

Here, $\lambda_P = \left(\sqrt{\nu_P^2 + 4D_P k_P} - \nu_P\right)/(2D_P)$. Some fraction of mRNAs may have 3′ UTR sequences that localize them to the soma (Tushev et al., 2018). In this case, the proteins emerging from the somatically localized mRNAs can be described by the following distribution:

$$P_{ss}^{\mathrm{som}}(x) = \frac{\beta_P\beta_R\lambda_P}{k_R k_P}e^{-\lambda_P x}. \qquad \text{(Equation 5)}$$

In a neuron, the dendritic protein distribution is determined by both somatically and dendritically synthesized proteins. Thus, the total distribution of protein is a mixture of the form $S_{\mathrm{mRNA}} \cdot z \cdot P_{ss}^{\mathrm{som}}(x) + (1 - S_{\mathrm{mRNA}}) \cdot P_{ss}^{\mathrm{den}}(x)$, whereby S_{mRNA} denotes the fraction of mRNAs found in the soma and z denotes the fraction of somatically synthesized proteins that is transported to the dendrite. Interestingly, our minimalistic model can already reproduce three fundamental types of protein distributions (Figure S5B): (1) monotonically decreasing protein concentration as a function of dendritic distance, (2) a local plateau in the vicinity of the soma followed by an exponential decrease toward distal sites, and (3) an increasing density of proteins at proximal and intermediate distances followed by a peak and decreasing density at very distal sites. Parameters for these three distribution types are given in the Supplemental Information. In Figure S7, we also mimic the atypical distribution of HCN-channels in pyramidal neurons. These channels have a high density in distal dendrites and a low density close to the soma. By introducing inhomogeneity in HCN-channels protein half-life, we obtained a distribution that increases with distance to the soma (Data S2).

Our next goal is to compare the theoretical predictions to our own experimental *in vitro* measurements of endogenous CaMKIIα mRNA and protein distributions. CaMKIIα is one of the most abundant proteins of the postsynaptic density (Kennedy et al., 1983) and a major player in the induction and maintenance of long-term potentiation (LTP) in synapses (Kennedy et al., 1983; Malenka et al., 1989; Chen et al., 2008). In fact, CaMKIIα knockout mice exhibit impaired performance on a spatial-memory task and dramatically reduced LTP in area CA1 of the hippocampus (Silva et al., 1992). Below, we adapt our model parameters for the protein of interest, CaMKIIα, either using our own experimental measurements or by deriving the parameters from literature.

We start with the transcription and translation rates (β_R and β_P). First, let us note that all normalized distributions we show are invariant with respect to the numerical values chosen for the translation and transcription rates. For the transcription rate of CaMKIIα, we calculated $\beta_R = 0.001$ mRNAs/s. To obtain this value, we considered that the CaMKIIα pre-mRNA is 101,892 nt long, the average mRNA elongation rate is 58 nt/s (Darzacq et al., 2007; Dundr et al., 2002), and two genes are available for transcription. The average translation rate measured experimentally is $\beta_P = 0.021$ proteins/s, which reflects the average ribosomal initiation rate per second (Wu et al., 2016). Next, we calculated the degradation rates of mRNAs and proteins (k_R and k_P) from their reported lifetimes using the relation $k = \ln(2)/T_{1/2}$, where $T_{1/2}$ denotes the half-life of the molecule. For CaMKIIα, the average mRNA half-life has been reported to be in the range of 8.5 h (Yang et al., 2003) to 20 h (Schwanhäusser et al., 2011; Tushev et al., 2018). We used a degradation rate of $k_R = 1.2 \times 10^{-5}$ mRNA/s, which corresponds to an average half-life of 16 h for the various mRNA isoforms of CaMKIIα (Tushev et al., 2018). The half-life reported for CaMKIIα proteins ranged from 4.14 days (Schwanhäusser et al., 2011) to 6.64 days (Dörrbaum et al., 2018). Here, we used the protein degradation rate of $k_P = 1.21 \times 10^{-6}$ proteins/s, which corresponds to the most recently reported half-life value of 6.64 days.

We next considered the mechanisms and speeds of movement of mRNA and protein within the cell. We summarize in Table 2 the range of reported diffusion coefficients and microtubule transport velocities obtained using a variety of experimental techniques, including ^{3}H-uridine pulse-labeling (Davis et al., 1990) and live tracking of GFP-labeled molecules (Park et al.,

Table 2. Reported Transport Parameters Measured in Dendrites of Hippocampal Cultured Neurons

	mRNA	Protein
Diffusion, $\mu m^2/s$	3.0×10^{-3}, nonspecific (Davis et al., 1990); 3.8×10^{-3}, β-actin (Park et al., 2014)	4.5, CaMKIIα (Khan et al., 2012); 0.023–0.254, CaMKII (Lu et al., 2014)
Velocity, $\mu m/s$	5.8×10^{-3}, nonspecific (Davis et al., 1990); 1.3, β-actin (Park et al., 2014)	0, CaMKIIα (Shen and Meyer, 1999; Hirokawa and Takemura, 2005)

We used these parameters in Figures 1 and 2.

2014). Overall, the velocities reported for active transport of mRNAs are in the range of 10^{-3} $\mu m/s$ to 1.0 $\mu m/s$ and the mRNA diffusion coefficients are on the order of 10^{-3} $\mu m^2/s$. The transport mode of a protein depends on whether it is a part of a large protein complex (e.g., part of a vesicle) or whether it is freely diffusing. As examples of diffusion coefficients for freely diffusing proteins, we used the numbers reported for CaMKIIα in dendrites that ranged from 4.5 $\mu m^2/s$ to 10^{-2} $\mu m^2/s$. The range of possible dendritic mRNA and protein distributions, as predicted by our theory, is presented in Figures 1C and 1D. To determine this range, we applied the smallest and the largest experimental values from Table 2 to our model predictions in Equations 2, 4, and 5. When estimating the upper limit for the mRNA distribution ($D_R = 3.8\times10^{-3}$ $\mu m^2/s$, $\nu_R = 1.3$ $\mu m/s$), we detected a saturation of mRNA levels when a dendritic distance of 100 μm was evaluated (Figure 1C, dark-blue line). With lower transport values ($D_R = 3.0\times10^{-3}$ $\mu m^2/s$, $\nu_R = 5.8\times10^{-3} \mu m/s$), we predicted an 18.7% decrease in mRNA across the same 100 μm length of dendrite (Figure 1C, light-blue line). Since the degradation rate was the same in both predictions, the difference in the basal distributions must be due to a variation in transport velocity and/or diffusion coefficient.

Given the difference in the predicted mRNA distributions, we next asked whether a similar variation exists for the protein distributions. If the concentration of mRNAs along the dendrite is constant, then barring any changes in the translational efficacy or increased proteolysis, we would expect a similar constant concentration of protein. But if distal locations of the dendrite exhibit reduced mRNA levels, as we predicted with the lower mRNA transport velocity and diffusion coefficient (Figure 1C, light blue line), would the basal protein distribution be similarly reduced? To determine the distribution of proteins along the dendrite as a function of distance from the cell body, we considered the parameters of the lower bound on the mRNA distribution that resulted in the light blue line in Figure 1C.

We found that the reduction in mRNAs could be compensated by a large protein diffusion coefficient ($D_P = 4.5$ $\mu m/s^2$, as reported by Khan et al. (2012). For this case, our model predicts an almost flat protein distribution across a 100 μm span of dendrite (Figure 1D, red line; 0.015% drop in protein compared to 18.7% drop in mRNA across 100 μm). Next, we asked whether a reduced diffusion coefficient, as reported by Lu et al. (2014) ($D_P = 0.023$ $\mu m/s^2$), could produce a noticeable drop in the protein concentration. We found that with this reduced motility of proteins, there was a 29% decrease in the protein concentration at 100 μm (Figure 1D, orange line). We note that the active velocity was set to zero, $\nu_P = 0$ $\mu m/s$, taking into account experimental reports that CaMKIIα protein behaves like a soluble protein (Shen and Meyer, 1999; Hirokawa and Takemura, 2005).

To test our model's predictions, we conducted experiments in cultured rat hippocampal neurons and measured the endogenous CaMKIIα mRNA and protein distributions. For the dendritic mRNA distribution, we used high-resolution fluorescence *in situ* hybridization (FISH) together with a MAP2 immunostaining to unambiguously distinguish between neuronal dendrites and other cellular compartments (Figures 2A and 2D, left). To assess the protein distribution, we used immunostaining with an anti-CaMKIIα antibody together with MAP2 immunostaining (Figures 2B and 2E). We found that CaMKIIα mRNA and protein were detectable throughout the proximal and distal dendritic compartments of hippocampal neurons, as previously reported (Cajigas et al., 2012; Tushev et al., 2018). To assess the spatial distribution of CaMKIIα mRNA, we assigned each detected mRNA puncta a dendritic distance. We then quantified the CaMKIIα mRNA distribution by creating a frequency histogram (bin width, 5 μm) of the mRNA puncta locations. Subsequently, we computed an average across the dendritic segments in our dataset, where each dendrite had a minimal length of 100 μm. To account for dendritic tapering away from the soma, we conducted additional model calculations (Data S3). The result of analysis motivated us to normalize the mRNA density by a measure that is proportional to the local dendritic radius rather than volume. Specifically, we normalized the mRNA density by the MAP2 intensity at the corresponding location (Figures S2 and S3) and then fitted the resulting endogenous mRNA distribution using Equation 2 for R_{ss}^{den} (Figure 2D). Interestingly, we found that the mRNA data and their exponential fit (gray dotted and black line) were consistent with the lower and upper bounds predicted by our theory. The exponent of the fit, $\lambda_R = 0.0018$ μm^{-1}, and its 95% confidence interval, $(0.0008,\ 0.0028)\mu m^{-1}$), allowed us to derive the mobility parameters that describe the measured CaMKIIα mRNA data. Here, we assumed an average diffusion coefficient $D_R = 3.4\times10^{-3}$ $\mu m^2/s$, and using both the mRNA degradation rate k_R and the fitted exponent λ_R, we determined an average transport velocity $\nu_R = 6.7\times10^{-3}$ $\mu m/s$. These values are within the range of reported trafficking parameters and characterize the statistical average of the endogenous distribution of CaMKIIα mRNA molecules. Measuring the average velocity of mRNA granules is challenging, because only a fraction of them is motile at any given time (Buxbaum et al., 2015). Therefore, it is interesting to ask whether the velocities measured for a subpopulation of mRNA granules are representative of the statistical average. The derived velocity, $\nu_R = 6.7\times10^{-3}$ $\mu m/s$, and its error, $\nu_R \in (0.004, 0.015)$, falls within the range of values reported for other mRNA species but is lower than the value reported for moving CaMKIIα mRNA granules (4.0×10^{-2} $\mu m/s$). This suggests that only a fraction (14%) of the CaMKIIα mRNA population is mobile at any given time.

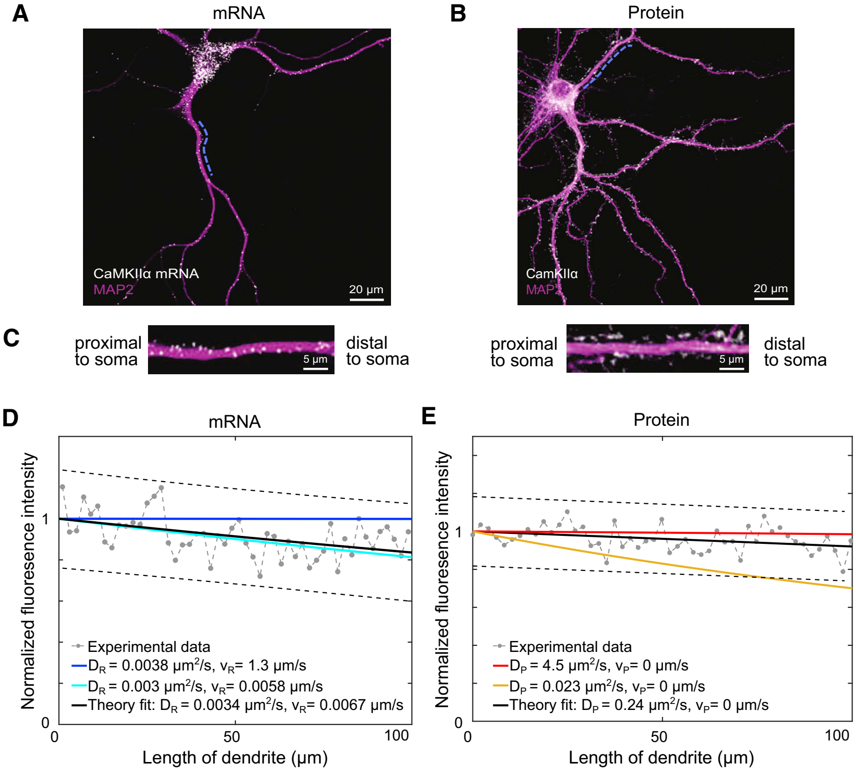

Figure 2. CaMKIIα mRNA and Protein Distributions in Cultured Neurons

(A) Representative image of high-resolution fluorescence *in situ* hybridization for CaMKIIα mRNA (white) in a cultured hippocampal neuron. MAP2 antibody (blue) labels the dendritic arbor.

(B) Sample image of CaMKIIα protein immunostaining (white) together with anti-MAP2 labeling (purple) to visualize the dendrites.

(C) Zoom-in of straightened dendrites from (A) and (B) (dashed blue lines).

(D) The distribution of CaMKIIα mRNA over a dendritic distance of 100 μm is shown (dotted, gray), along with the mRNA upper and lower (solid dark blue and light blue) boundaries from Figure 1C and a fit of the experimental data (solid, black) using the function in Equation 2.

(E) Experimental data for CaMKIIα protein (dotted, gray) is shown along with the upper and lower boundaries from Figure 1D (solid red and gold) and a fit of the experimental data (solid, black) using the functions in Equations 4 and 5 and mRNA parameters from (D).

Next, we compared our theoretical prediction for the distribution of the proteins with the experimentally measured fluorescence intensity distribution of endogenous CaMKIIα protein in dendrites. To account for any proteins located in spines and any change in dendritic radius and spine volume across distance, we normalized the protein intensity distribution by an area mask that comprised the dendritic and spine areas (Figure S1). We fitted the resulting endogenous protein distribution using the P_{ss}^{den} and P_{ss}^{som} in Equations 4 and 5. From the fit, we determined the free protein transport parameters and set the mRNA related parameters to values corresponding to the mRNA data in Figure 2D. We set the fraction of somatic mRNAs to $S_{\mathrm{mRNA}} = 0.557$ in agreement with our results (Figure 4). The gray dotted line represents the normalized protein fluorescence, while the black line is the corresponding theory fit of the data (Figure 2D); the red and gold lines are the upper and lower bounds from Figure 1C derived from experimental reports. Interestingly, we found that the protein distribution is nearly constant across a dendritic distance of 100 μm, and the fit of the experimental data revealed the exponent $\lambda_P = 0.00223\ \mu\mathrm{m}^{-1}$ with the 95% confidence interval $(0.00086,\ 0.0036)\ \mu\mathrm{m}^{-1}$. From this, we derived a mean diffusion coefficient, $D_P = 0.24\ \mu\mathrm{m}^2/\mathrm{s}$, and its error, $D_P \in (0.09, 1.63)\ \mu\mathrm{m}^2/\mathrm{s}$. This value is in good agreement with the diffusion coefficient $D_P = 0.254\ \mu\mathrm{m}^2/\mathrm{s}$ reported for a large dendritic population of fast CaMKII molecules (Lu et al., 2014).

Dissecting the Role of mRNA Diffusion, Active Transport, and Half-Life

Our next goal was to understand how the mRNA and the protein distributions are shaped by the mRNA transport velocity ν_R, diffusion coefficient D_R, and degradation rate k_R. This raises the question how these parameters shape not only the distribution of mRNA in the dendrite but also the protein concentration. First, we addressed the impact of the mRNA transport velocity ν_R on the mRNA and protein distributions by up- or down-scaling of mRNA velocity ν_R relative to the baseline value that we obtained in Figures 2D and 2E while keeping all other parameters constant. Surprisingly, we found that just a 5-fold decrease in the mRNA velocity $(\nu_R/5)$ strongly affected both the mRNA and protein distributions (Figures 3A and 3B) by dramatically increasing the amount of proximal mRNA while lowering the amount of distal mRNA. Inversely, if the mRNA transport velocity was increased 2-fold $(\nu_R \times 2)$, our model predicted a more homogeneous mRNA distribution along the dendrite (Figure 3A). In our model, modifications to the mRNA transport velocity do not change the overall amount of mRNA and protein molecules in the dendrite, but they modify the way in which they are distributed along the dendrite. Changes in the mRNA velocity induced similar changes in protein distributions; a lower ν_R resulted in a higher protein concentration at proximal sites, and a higher ν_R led to a more homogeneous protein distributions across the dendrites (Figure 3B). Interestingly, we found that the mRNA and protein distributions are far less sensitive to modifications of the mRNA diffusion coefficient D_R when compared to ν_R. Only large 100- or 1,000-fold changes in D_R induced noticeable modifications in the spatial distribution of mRNA or proteins (Figures 3C and 3D). For example, it was necessary to increase the mRNA diffusion coefficient 1,000-fold in order to achieve a protein distribution shift comparable to the effect induced by the 2-fold increase in the mRNA velocity. Similarly, even a 100-fold decrease in the mRNA diffusion coefficient did not lead to any noticeable changes in either mRNA or the protein profile. Taken together, these observations indicate that the modulation of active microtubule-mediated transport

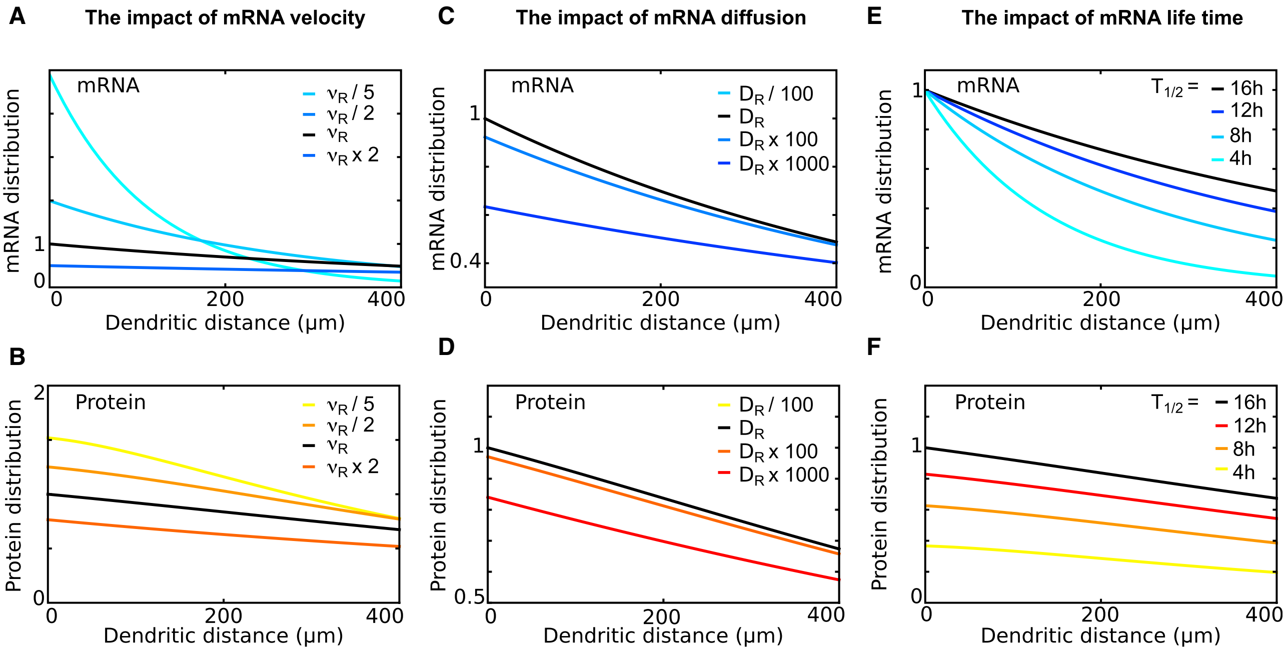

Figure 3. Changes in mRNA Half-Life and Its Transport Velocity Can Significantly Change the Dendritic Protein and mRNA Distributions

Starting from the experimentally measured mRNA transport parameters (Figure 2) ($D_R = 3.4\times10^{-3}\ \mu m^2/s$, $\nu_R = 6.7\times10^{-3}\ \mu m/s$), we up- or downscaled these transport parameters to see how susceptible the mRNA and protein distributions are to changes in these values.

(A and B) Changing the mRNA transport velocity had a dramatic effect on the mRNA distribution (A), while the corresponding protein distributions experienced the largest changes at distal sites (B).

(C and D) If the diffusion coefficient is increased by 100- or 1,000-fold, then the largest change to the mRNA distribution occurs (C). Similarly, the protein distribution only changes when the mRNA diffusion coefficient is increased 100- and 1,000-fold (D). Reductions in the diffusion coefficient, 100- and 1,000-fold, resulted in mRNA (yellow) and protein (light blue) distributions that overlapped with the original black line.

(E and F) With a lower half-life, mRNA distribution decays faster (E), and consequently, the amount of protein decreases for distal sites (F).

In all panels, we normalized all distributions by the value of the original protein distribution in the origin to visualize differences in the relative number of molecules. Alternative normalization strategies are explored in Figure S4.

of mRNAs rather than mRNA diffusion is an efficient way to regulate the amount of mRNA and proteins available across the dendrite.

Manipulating the mRNA half-life by modulating k_R, had a direct influence on both the mRNA and the protein distributions. When the half-life of the mRNA molecules in the cytoplasm was reduced from 16 h to 4 h, the mRNA concentration exhibited a steeper decay from proximal to distal sites, such that the relative drop was ~40% larger. The reduction of mRNA half-live also resulted in a severe drop in protein distributions, where ~50% less protein was delivered to distal sites for a 4 h half-life in comparison to a 16 h half-life. This shift hints at the possibility that the dendritic mRNA population, which determines the amount of local versus somatic translation, can substantially alter the amount of locally available proteins. Recently, we showed that mRNAs located in neuronal dendrites tend to carry longer isoforms of 3′ UTRs and have longer half-lives (Tushev et al., 2018). Such variations in mRNA half-lives could be easily implemented in the model by introducing the different values in Equations 4 and 5, which describe proteins made from dendritic and somatic mRNAs, respectively. As shown in Figure S5A, if dendritic mRNAs have a two times longer half-life than somatic ones, it leads to a 11% increase in CaMKIIα proteins in the dendrite at 400 μm (see also Supplemental Information). Although we focus on CaMKIIα mRNA and protein distributions in Figure 3, we also offer our readers the possibility to explore other mRNA or protein species.

Revealing the Role of Somatic versus Dendritic mRNA for the Dendritic Protein Profile

Our next goal was to understand how somatic and dendritic mRNAs shape the distribution of proteins in the dendrites. While some mRNAs move out into the dendrites, some stay in the soma, because they lack specific features in their 3′ UTR localization sequence or have sequences that give rise to their active retention in the soma. For instance, CaMKIIα mRNA possesses multiple 3′ UTR variants (Tushev et al., 2018) that contain or lack localization elements as well as other regulatory elements (Tian and Manley, 2017; Mayford et al., 1996; Hilgers et al., 2011). CaMKIIα mRNAs lacking a specific 3′ UTR localization element remain primarily in the neural somata (Mayford et al., 1996; Tushev et al., 2018). To incorporate this into our model framework, we need to determine the fraction of the mRNAs that migrate into the dendrites and the fraction of the dendritic proteins that originate from somatic rather than dendritic mRNA. To obtain this information directly, one would need to

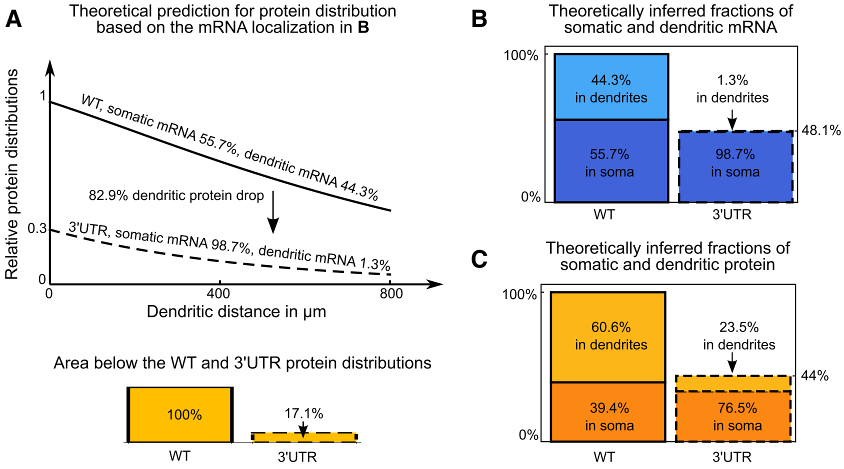

Figure 4. The Model Highlights the Advantages of Dendritic mRNA in Providing Proteins to Distal Dendritic Sites

(A) Using our model, we derive the dendritic protein distributions in WT and 3′ UTR mutants based on the mRNA localization patterns in (B), which we inferred from the experimental results in Miller et al. (2002). Note, that the point $x = 0$ in the model represents the soma border and is part of the dendritic statistics; the soma is represented by a separate compartment in our model. Consistent with the theoretically inferred fraction of somatic and dendritic protein, our model predicts an 82.9% dendritic protein drop after 3′ UTR deletion.

(B) From the relative mRNA decrease in the soma and dendrites reported in Figure 2 in Miller et al. (2002), we inferred that in the WT, 55.7% of mRNAs are located in the soma and 44.3% in dendrites. Consistent with Miller et al. (2002), the overall number of mRNAs after 3′ UTR deletion drops to 48.1% relative to WT in our model.

(C) We inferred the relative protein amounts in WT and 3′ UTR mutants from data reported in Miller et al. (2002). Interestingly, after the removal of almost all dendritic mRNA, the dendritic protein count did not drop to zero; ~17% of the WT protein count remained in the dendrites, which allowed us to determine the amount of somatically generated proteins that move into the dendrites.

label and monitor all proteins and mRNAs individually to determine their origins and their final localizations. However, it is also possible to infer this information from available experimental evidence. To this end, we reanalyzed the data in the seminal Miller et al. experiment (Miller et al., 2002). We were able to calculate the fraction of CaMKIIα mRNA localized in dendrites and the fraction dendritic CaMKIIα proteins that were synthesized from mRNA localized in the soma.

We start by inferring the relative distribution of CaMKIIα mRNAs between soma and dendrites. The study (Miller et al., 2002) reports that after the deletion of the 3′ UTR localization sequence, the total mRNA count was reduced to 48.1% relative to wild-type (WT), whereas dendritic and somatic mRNAs were reduced to 1.4% and 85.3%, respectively. From this, we inferred that in the WT 55.7% of all mRNAs are in the soma, while 44.3% are distributed throughout the dendrites. This is a remarkable finding because it means that close to half of CaMKIIα mRNAs are trafficked out of the soma and ultimately lead to a large amount of protein synthesized directly in dendrites. Here, we briefly summarize the steps we took to arrive at this soma-to-dendrite mRNA ratio and present a more detailed derivation in Data S4.

We assume that in the WT neurons the total mRNA count is T and it is distributed between the soma region (S) and the dendrites (D). The fraction of mRNA in the soma is S/T, and the fraction of mRNA in the dendrites is D/T. Using the information from the Miller et al. article, we find that the amount of mRNA in the mutant satisfies the following relation $0.481 \cdot T = 0.853 \cdot S + 0.014 \cdot D$ and the WT mRNA amount satisfies $S/T + D/T = 1$. These two equations have a unique solution, which is $S/T = 0.557$ and $D/T = 0.443$. Analogously, one can compute the fraction of somatic and dendritic mRNAs in mutants as 0.987 and 0.013, respectively. Interestingly, if the removal of the 3′ UTR localization sequence would not alter any other property of the mRNAs except to prevent their translocation into the dendrite, we would expect that the total amount of mRNA stays the same resulting in a roughly 2-fold increase in the soma. However, a previous study indicates that 3′ UTR sequences, including those of CamKIIα mRNAs, are important for mRNA stability (Tushev et al., 2018). In fact, the total mRNA count in the CamKIIα 3′ UTR mutants is reduced by 51.9%. We hypothesize that this drop can be explained by a reduction in the CamKIIα mRNA half-life. Indeed, our model predicts that a 51.9% reduction of the mRNA half-life can be accounted for the drop in the total mRNA count and the resulting reduction in total protein amount (Figure 4A).

The rate at which protein is synthesized from mRNA is known as the translational efficiency. Translational efficiency is influenced by the number of ribosomes loaded onto an mRNA, the RNA structure, and any *cis*- and *trans*-regulatory elements present in the mRNA. We considered next the translation efficiency of the soma and the dendrites, calculating their ratio. To this end, we assumed that all proteins emerged either from somatic or dendritic mRNAs, and we accounted for the possibility that the translation efficiency in the soma and dendrites may be different. We denote the translation efficiency ratio between dendrites and soma by T_R, such that for each protein produced by a somatic mRNA, there are T_R proteins produced by a dendritic mRNA. Using the relative ratio of somatic and dendritic mRNA from above, we obtain the equation $0.557 \cdot T + T_R \cdot 0.443 \cdot T = P$, which determines the total protein count P in the WT relative to the total mRNA count T. Using the information about the total and the relative protein drop in the dendrites after the 3′ UTR deletion, we obtain a second equation $0.987 \cdot (T \cdot 0.481) + T_R \cdot 0.013 \cdot (T \cdot 0.481) = P \cdot 0.44$. Here, 0.987 and 0.013 represent the fractions of somatic and dendritic mRNAs in the mutants. Solving these equations, we arrive at the finding that the translation ratio is $T_R = 1.22$. This indicates that each dendritic CaMKIIα mRNA synthesizes ~20% more CaMKIIα proteins than the ones located in the soma.

In the next step, we infer the fraction of proteins generated in the soma that move into the dendrites, denoted by z. In order to obtain z, we use information about the relative mRNA localization and the relative translation ratio between soma and dendrites in the WT and the 3′ UTR mutant described by Miller et al. In the WT, the dendritic proteins comprise a fraction that originated from dendritic mRNA $(D \cdot T_R)$ and a fraction that originated from somatic mRNA $(S \cdot z)$; together, this constitutes the total protein count in the dendrites $S \cdot z + D \cdot T_R = P_D$. After the 3′ UTR deletion, the somatic and dendritic mRNA dropped to 85.3% and 1.4% of their WT value, respectively. The dendritic protein count in the 3′ UTR mutant was 17.1% of its WT value. From these relations, we obtain a second equation, $0.853 \cdot S \cdot z + 0.014 \cdot D \cdot T_R = 0.171 \cdot P_D$. Taken together both relations imply that the fraction of somatically generated proteins in the dendrites is $z = 0.22$ (Figures 4B and 4C). Additionally, we obtain the relative amounts of the dendritic and somatic proteins in a WT neuron, which are 60.6% and 39.4%, respectively. Notably, while only 44.3% of total CaMKIIα mRNAs localized to the dendrites, this still resulted in a substantially higher percentage (60.6%) of CaMKIIα proteins being localized in this compartment. Interestingly, based on the inferred values for the translation efficiency and the mRNA soma-dendrite distribution, our model reproduced the reduction in total protein amount (area under the curve) in the 3′ UTR mutants relative to WT (89.2%) reported by Miller et al. (Figure 4A).

We summarize the results of our analysis in Figures 4B and 4C. Overall, we learned from this analysis that modifications of 3′ UTR sequences can be a useful tool for dissecting the localization and motility profile of mRNAs and proteins in neurons. It also suggests that behavioral effects attributed to 3′ UTR modifications can have multiple competing explanations. They can either result from changes to the total mRNA and protein count or from modifications of the relative distribution of mRNAs and proteins between soma and dendrites or within dendrites.

How New mRNAs and Proteins Populate the Dendrite

The lifetimes of mRNAs and proteins are finite and many orders of magnitude shorter than the lifetime of a neuron. It is thus necessary for a neuron to constantly produce new molecules to replace those that were degraded. For example, the typical half-life of a CaMKIIα mRNA is ~16 h (Tushev et al., 2018), which means that after ~1.5 days, more than 80% of the mRNA in the dendrite has been degraded and needs to be replaced to keep the dendrite functional. Similarly, the half-life of CaMKIIα protein is ~6.64 days (Dörrbaum et al., 2018), which means that 80% of proteins will have decayed after ~15 days and need to be replaced. It is worth noting that under basal conditions (ongoing network activity in the absence of an external stimulus), there is ongoing transcription to match the rate of mRNA degradation in both the soma and dendrites. But what are the spatial and temporal dynamics of this turnover, and how do new molecules populate dendrites?

Recent experiments, using metabolic labeling to visualize newly synthesized RNA molecules, indicate that it can take up to 3–6 h for newly synthesized mRNAs to reach a distance of 150 μm (see Figure 1D in Akbalik et al., 2017). This is a remarkably long timescale, which is comparable to the lifetime of the mRNAs themselves. Interestingly, *in situ* experiments using bioorthogonal non-canonical amino acid tagging (BONCAT) and immunolabeling show that the dynamics of newly synthesized proteins is fundamentally different and that their concentration increases simultaneously across different dendritic locations (see Figure 4D in Dieterich et al., 2010). To understand these findings, we used our model to calculate the spatial profile of the newly synthesized mRNAs and proteins evolving in time using the mRNA and protein parameters that we obtained previously for CaMKIIα. Details of the mathematical derivations can be found in STAR Methods.

To mimic the experiments, we determined the location of all mRNAs that were produced from $t = 0$ onward. Since the mRNAs were transcribed in the soma, at $t = 0$ there were no labeled dendritic mRNAs. With time, newly transcribed mRNA appeared in the soma and subsequently translocated throughout the dendrite via diffusion or active transport. Over the course of a few hours, a moving front of new mRNAs appeared in the dendrites and after ~20 h, it reached an equilibrium within the displayed 400 μm dendritic segment where decay, synthesis, and transport balanced out (Figure 5A). This mRNA equilibrium was characterized by an exponential distribution, whereby the maximum amount of mRNA was located in the soma (Figure 5B).

We next reconstructed the dynamics of newly synthesized proteins and isolated the contributions of somatic and dendritic translation. We found that unlike the mRNA dynamics, a clear wavefront in the distribution of protein over time was not observed (Figures 5C–5F). We compared the distance covered by somatically synthesized proteins alone to the situation where somatic and dendritic mRNAs are translated. As expected, we found that somatic proteins did not populate distal dendritic compartments as rapidly as in the case of simultaneous dendritic and somatic translation (inset to Figure 5). We note that at distal sites, the concentration of newly synthesized proteins produced in the dendrites rose quickly (within the first minutes) and that their concentration across the whole dendrite rose almost simultaneously with time (Figure 5B). Moreover, both model predictions were in line with previous experiments (Akbalik et al., 2017; Dieterich et al., 2010).

Overall, our results indicate that the CaMKIIα mRNA basal distribution is reached quickly (after ~20 h) when compared to the 30 days it takes new proteins to populate the dendrite (Figure 5). This can be explained by the difference in the molecule's half-lives and their production sites. Notably, neurons in cultures have been reported to grow their dendritic arbors until 3–4 weeks. After this growth period, the dendritic arbor remains very dynamic, but growing and retracting branches balance out (Zhao et al., 2006; Kaech and Banker, 2006; Koleske, 2013). This is in line with our model predictions that show a timescale of several weeks (~30 days) to reach the equilibrium of the protein distribution of CaMKIIα (Figure 5).

What implications do the dynamics of newly synthesized proteins have for proteostasis? If we consider that a dendritic compartment may, for example, have a 10% higher baseline protein demand after plasticity induction, then how fast might this increase be implemented? Our results suggest that it would take many hours or even days to establish a new, higher protein level across all dendritic sites (Figures 5C and 5E). The recruitment of new proteins seems to be a very slow process that is at odds with brief, local changes in the protein amount. However,

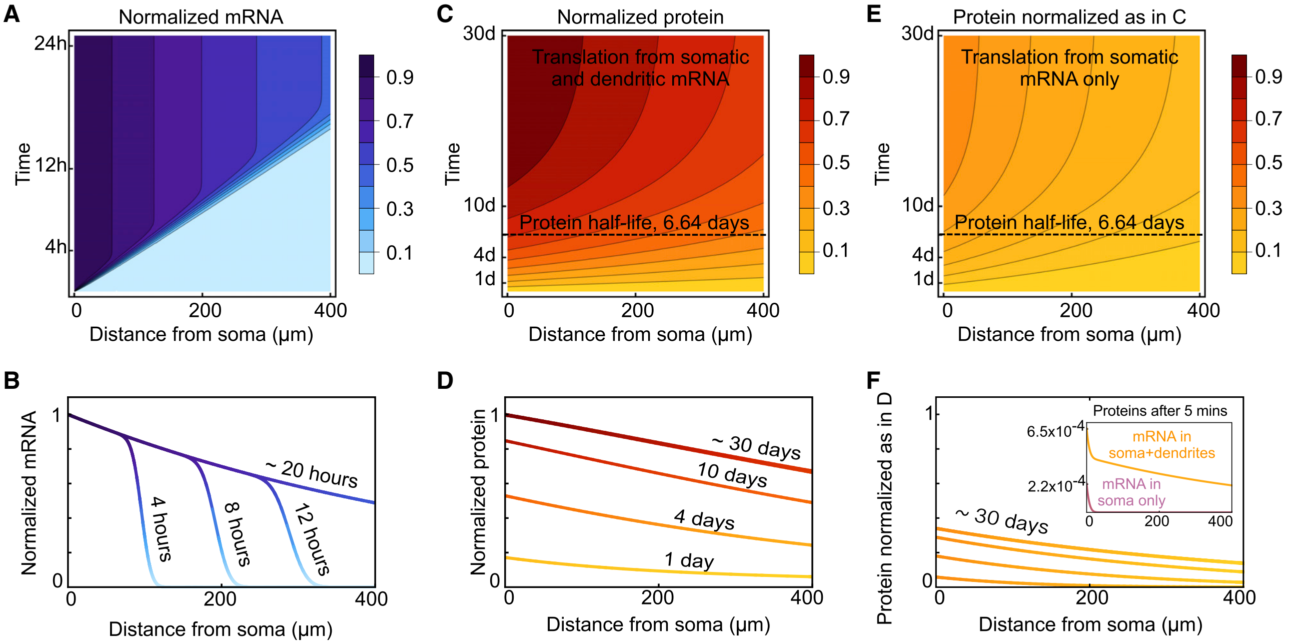

Figure 5. Using a Model to Reveal How New mRNAs and Proteins Populate a Dendrite

(A and B) The newly transcribed mRNA molecules emerge from the soma and subsequently populate the dendrite (A). En route, the mRNA diffuses, is transported along microtubules, or decays. After ~20 h, the spatial distribution reaches its equilibrium, where decay, production, and movement balance out (B).

(C and D) Newly synthesized proteins emerge from dendritic and somatic mRNA and populate the dendrite (C). The dendritic mRNA contributes to a quick rise in protein at distal sites (D), zoom into short time scales (F, inset). The protein reaches its steady state after ~30 days (D).

(E and F) Emergence of protein from somatic mRNA (E) is characterized by a quicker rise in protein at proximal sites but a slower increase in protein concentration at distal sites (F). The inset in (F) compares the protein distributions with and without dendritic mRNA present 5 min after onset.

global changes in translation are only one solution to serve increases in protein demand; an alternative way could be to locally induce a brief increase in translation, a "translational burst."

Impact of a Local Translational Increase

How does the induction of a local translational burst change the distribution of proteins around the stimulated site? To understand the resulting translational activation profile recently observed in an *in vitro* study of neurons (Wu et al., 2016), we applied a translational burst involving a single mRNA at the dendritic distance of 300 μm. The burst lasted for ~15–20 min, had a peak translational rate of 2.1 proteins/min (0.035 proteins/s), representing a 67% increase in the basal rate of protein synthesis, and covered an area of 1–2 μm (Figure 6A) which corresponds, approximately, to the diameter of a synaptic spine (Harris and Weinberg, 2012). We observed that ~10 min after the translational burst was initiated, the protein concentration reached its maximum at the stimulated site and that ~1 h after the burst, the total number of newly synthesized proteins reached its maximum (Figure 6B). The peak of the translational burst is denoted by a white cross (Figures 6A and 6B). Thus, our model predicts that the peak translational burst and the peak of the protein response are not simultaneous, but the protein response lags by ~10 min. Strikingly, this prediction fits the experimental observation that optogenetic stimulation of spines leads to an increase in CaMKIIα protein concentration that reaches a maximum after 10 min (600 s) (Zhang et al., 2008). Despite the fact that the translational burst lasted only 15 min, the distribution of newly synthesized proteins spread across the dendrite on a timescale of hours. Approximately 2 h after the stimulation, the newly produced proteins covered a distance of 100 μm. Importantly, dendritic locations that were further away from the site of stimulation (>100 μm) were not significantly altered by the translational burst. These data indicate that if the translational burst of the same size and duration takes place in the soma, then the plasticity-induced demand at distal sites cannot be met (Figures 6C and 6D).

In summary, our results indicate that the translational increases induced by one synapse can spill over and increase the availability of the corresponding proteins at neighboring dendritic sites because the spatial extent of protein response to a brief and local translational burst can affect an area of ~100 μm around the stimulation site (Figure 6). In addition to transient translational bursts, synaptic spines can also introduce long-term changes to the dendritic protein profile by siphoning off proteins from the dendrite through the spine neck. This flow can be represented by a local negative source term (see Supplemental Information) and can alter the protein concentration within a radius of up to 100 μm around the spine. The amplitude and the spatial range of this spine-induced change in protein concentration depend primarily on the protein diffusion coefficient and the strength of the flux into the spine (Figure S6 and Data S1). In pyramidal neurons, the spine density is low (~1 spine/μm) (Fiala and Harris, 1999), such that effects of spines

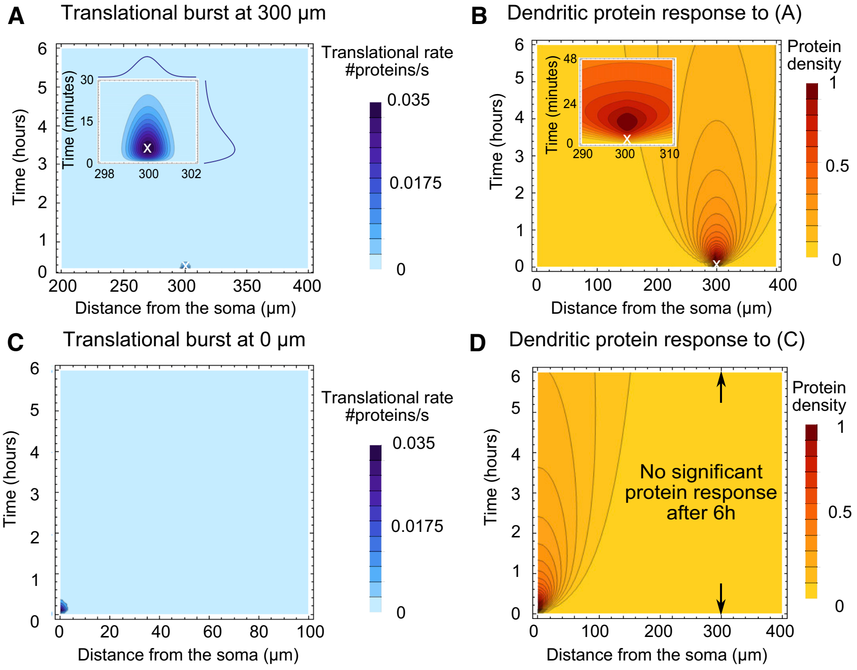

Figure 6. Predicting the Protein Response to Brief Local Translational Bursts

(A and B) Upon the introduction of a local increase in translation at a dendritic distance of 300 μm (A), our model predicts the corresponding protein response (B). We found that the protein response had a large spatial extent almost 20 times larger than the area that upregulated translation during the burst. Furthermore, the protein response endured almost 10 times longer than the translational burst by which it was triggered.

(C and D) The same translational burst acting at the soma (C) did not significantly affect dendritic protein count at the site of interest, which is greater than 100 μm away from the soma (D). To raise the protein count at dendritic sites, somatic translational bursts need to last longer than their dendritic counter parts or induce a larger translational increase.

stay local and do not alter the nature of the global diffusion dynamics described in the present study (see Figure 3 in Santamaria et al., 2006).

DISCUSSION

Here, we present a model incorporating both somatic and dendritic mRNA and protein sources that elucidates the temporal and spatial dynamics governing their active populations in dendrites. In the design of our model, we followed a data-driven approach by incorporating the available data on degradation, mRNA, and protein trafficking as well as translation dynamics. Our model makes predictions about the density of proteins and their corresponding mRNAs as a function of dendritic distance. These quantities are directly proportional to the respective average copy numbers per dendritic location that can be obtained from dendritic *in situ* experiments. By comparing the predicted density at two sites of interest, $P(x_1)$ and $P(x_2)$ or $R(x_1)$ and $R(x_2)$, one can gain intuition about the ratio between the average copy numbers at these sites. The relative error in the measurement of the average copy number is proportional to the inverse square root of the total molecule count. This would further imply that protein or mRNA species with a low total count can have a large fluctuation around the predicted average, while the more abundant species can be expected to have less error around the mean.

Because of the challenging nature of quantitative measurements in subcellular compartments, it remained elusive what fraction of mRNAs localizes to dendrites and how they determine the timescale of protein response and spatial dynamics. Using data from Miller and colleagues, we quantified the dendritic localization profile of CaMKIIα mRNAs and proteins. Our calculations show that while ~45% of all CaMKIIα mRNAs are localized to dendrites, more than ~60% of the whole CaMKIIα protein pool is localized in this subcellular compartment (Figure 4). The analysis of CaMKIIα 3′ UTR mutant mice was a useful tool to dissect the localization and motility profile of CaMKIIα mRNAs and proteins in neurons. Interestingly, CaMKIIα 3′ UTR mutant and heterozygote CaMKIIα knockout mutant mice have very comparable mild hippocampal-dependent memory impairments (Chen et al., 1994; Miller et al., 2002). Since both mutations lead to a significant decrease in both CaMKIIα mRNAs and proteins it is unclear whether the memory defects in CaMKIIα 3′ UTR mutant mice are due to the observed mRNA mislocalization or the overall reduction in protein level. However, our results suggest that a large decrease in dendritic mRNA levels will impair local production of CaMKIIα in dendrites (Figure 6). Thus, the memory impairments in both mutants could result from a failure to efficiently produce CaMKIIα in dendrite upon activity.

Most previous work (Bressloff and Earnshaw, 2007; Williams et al., 2016) assumed a central protein source at the cell body and disregarded the dendritic mRNA distribution. While this may be a good assumption for some proteins whose mRNAs are confined to the cell body, the mRNA for many neuronal proteins is clearly present in dendrites. In fact, over 2,500 different mRNA species localize into dendrites and/or axons (Cajigas et al., 2012). Our model captures this biological observation and can reproduce a large range variety of dendritic mRNA and protein distributions that can be explored and visualized using our web applet. An important consequence of the dendritic mRNA distribution is the ability to locally produce new proteins. Our model can now predict the spatial and temporal spread of these locally newly synthesized proteins. Previous models predicted delays of many hours or even days to match newly arising demand within 10% accuracy, while our model predicts that extra demand for proteins at distal sites can be addressed within a few minutes (10 min; see Figure 6). This is in line with experimental observations (Zhang et al., 2008; Govindarajan et al., 2011).

Our model predicts that the spatial mRNA profile can be described by an exponential function whose exponent is a function of the half-life, diffusion, and active mRNA velocity (see Equation 2). Interestingly, we found that modest 2- or 5-fold changes in the active transport velocity have a dramatic impact on the availability of proteins in distal compartments. On the contrary, increasing even 100-fold the diffusion coefficient has a very mild effect on protein distribution. This suggests that mutations affecting mRNA transport, as found in diseases like spinocerebellar ataxia, Huntington's, or amyotrophic lateral sclerosis (Hirokawa et al., 2010), are likely to result in dramatic changes in the availability of proteins across the dendritic tree. Similarly, we observed that large and global changes in protein localization could be induced by modulating mRNA degradation rate. This constitutes a relatively unexplored field in the context of neurons and plasticity. Recently, we found that dendritic mRNAs tend to have longer half-lives (Tushev et al., 2018). Indeed, our model suggests that fast and local modulation of mRNA half-life could be a critical point of regulation for synaptic plasticity.

Notably, our simple model reproduces three fundamental protein distributions: (1) monotonically decreasing protein concentration as a function of dendritic distance (e.g., the case of CaMKIIα), (2) a local plateau in the vicinity of the soma followed by an exponential decrease toward distal sites (e.g., the case of proteins with mRNA confined in the soma) and (3) an increasing density of proteins at proximal and intermediate distances followed by a peak and decreasing density at very distal sites (e.g., the case of proteins with short half-life, active protein transport and dendritic mRNA). We were also able by introducing a distance dependent protein half-life (Bingol and Schuman, 2006) to reproduce the atypical distribution of HCN channels in CA1 pyramidal neurons. We postulated that HCN channel mRNA is mainly confined to the soma and that the protein is longer lived in the distal dendrites. We obtain distribution where HCN channel density is increasing with distance to the soma as previously reported (Magee, 1998).

Our results also offer mechanistic insights into the mRNA and protein turnover processes in dendrites. Since mRNAs typically exhibit half-lives in the range of hours and proteins in the range of a few days, a neuron needs to constantly replace the decaying molecules. Newly synthesized mRNAs move into the dendrites on the timescales of hours (Akbalik et al., 2017). Our theory suggests that this movement can be described by a moving front, whose speed is determined by the average velocity of the active transport. For CaMKIIα this speed is 24.12 μm/h. Notably, our results indicate that it takes ~1 day to replace the dendritic mRNA population with new molecules. For newly synthesized proteins, our theory predicts a fundamentally different movement pattern across time and space. We found that the concentration of newly synthesized proteins is primarily determined by the long-range movement properties of proteins (Figure 5). This explains how the concentration of newly synthesized proteins can rise in unison across the whole dendrite as reported in experiments (Dieterich et al., 2010).

Given the slow dynamics of turnover processes, which plays out on the timescales of hours and days, we wondered how a local change in translation could affect the dendritic protein population. Our results demonstrate that a brief translational burst of a single mRNA species in dendrites changes the protein concentration at the site of stimulation 15 min after its onset (Figure 6). Interestingly, a comparable delay of several minutes was reported between spine stimulation and CaMKIIα accumulation peak (Zhang et al., 2008). This suggests CaMKIIα proteins accumulating in spines after LTP induction are at least in part locally newly synthesized. Also, our model provides a quantitative description of local translation bursts across short and long timescales. Interestingly, we found that the protein concentration can be elevated for up to 6–10 h after the translational burst. The proteins produced during the burst slowly redistribute over time so that only synapses within a 100 μm radius can potentially sense a local change in protein concentration. This is in line with the experimental observation that protein synthesis can spread 70 μm from the site of stimulation (Govindarajan et al., 2011; Rangaraju et al., 2019). At the same time, we found that somatic translational bursts of CaMKIIα mRNA do not affect distal sites due to the limited motility of the proteins (passive diffusion only). This finding suggests that dendritic plasticity that requires rapid changes to the proteome is accomplished by local rather than somatic translation.

In our present work, we coupled the local availability of CaMKIIα mRNA to the local synthesis of CaMKIIα proteins in the dendrite. Admittedly, this coupling only roughly summarizes the action of many cofactors involved in translation repression or activation of CaMKIIα mRNA. We recognize that translation is a complex process. But rather than modeling each individual cofactor, here, we chose to apply an average translation rate measured experimentally in neurons (Wu et al., 2016). While our average rate likely encompasses many of the different molecular interactions necessary for protein synthesis, it does not differentiate the individual steps or molecular regulations. One intensively studied mechanism of translation repression is the binding of FMRP (an RNA-binding protein involved in fragile-X syndrome) to a number of dendritic mRNAs such as CaMKIIα, Arc (also known as Arg3.1), or MAP1B (Zalfa et al., 2003). Future iterations of the current model can incorporate translational regulators like FMRP as more information about their kinetics emerges. Similarly, this study is primarily focused on cytoplasmic proteins; however, our theory can be also used to gain intuition about the motion of transmembrane proteins such as neurotransmitter receptors (Choquet and Triller, 2013). The endo- and exocytosis of protein-containing vesicles and the subsequent diffusion of these proteins along the dendritic surface can be approximated in our model by considering (1) active transport in the cytoplasm and (2) an additional diffusion term for the diffusion in the plasma membrane. While the kinetics of endo- and exocytosis rates remains largely unknown, our model can help building intuitions about how the different processes may influence the outcome distribution of a transmembrane protein of interest.

State-of-the-art experimental methods now allow recording the location of dendritic mRNAs and proteins in endogenous *in vitro* conditions as well as mRNA and protein dynamics in response to perturbations (Glock et al., 2017). As more information is collected, it will allow fine-tuning and generalizing of our model. For example, measuring endogenous mRNA distribution in experiments and comparing the outcome protein distribution to different model scenarios will help identify critical model ingredients (e.g., determine whether active transport of molecules is necessary to explain the experimentally measured distributions).

In summary, our work provides a unique perspective on the trafficking dynamics of mRNAs and proteins that is both mathematically rigorous and data driven. Although we focused on CaMKIIα both in our model parameters and in experiments, our model predictions can be easily generalized for any protein of interest. To facilitate this, we provide a web-based applet where our readers can adapt parameters and explore the resulting dynamics for other molecules of interest (see STAR Methods; http://www.tchumatchenko.de/Visualisation.html). Future studies can extend our theoretical framework further by including for instance anomalous diffusion (Equation 73 in Metzler and Klafter, 2000) in order to describe molecular dynamics in neurons with a high spine density (Santamaria et al., 2006; Pfeiffer et al., 2018). Our results suggest that active transport of mRNAs and/or proteins has major impact on protein steady-state distribution. Future models that incorporate spatial variability in microtubule-associated velocities such as arresting behavior in the vicinity of activated spines could help further our understanding of how neurons match protein demands upon synaptic plasticity.

STAR★METHODS

Detailed methods are provided in the online version of this paper and include the following:

- KEY RESOURCES TABLE
- LEAD CONTACT AND MATERIALS AVAILABILITY
- EXPERIMENTAL MODEL AND SUBJECT DETAILS
    - Hippocampal neuron preparation
- METHOD DETAILS
    - Methods for *in vitro* measurements of CaMKIIα mRNA and protein
    - Deriving the spatiotemporal mRNA dynamics
    - Deriving the spatiotemporal protein dynamics
    - Deriving the response to translational bursts
    - Mathematical details on functions E_{erf} and E_{erfc}
    - Mathematical details on integrals $\int v^{\eta} e^{-Av-Bv^{-1}} dv$
    - Mathematical details on inverse Laplace transforms
    - Solution of the diffusion equation

SUPPLEMENTAL INFORMATION

Supplemental Information can be found online at https://doi.org/10.1016/j.neuron.2019.06.022.

ACKNOWLEDGMENTS

We thank Ina Bartnik, Nicole Fürst, Anja Staab, Christina Thum, and Dirk Vogel for help with cell culture preparation and members of the Schuman and Tchumatchenko labs for fruitful discussions. This work was funded by the Max Planck Society and the German Research Foundation (CRC 1080; T.T. and E.M.S). This project has received funding from the European Research Council (ERC) under the European Union's Horizon 2020 research and innovation program (E.M.S. grant agreement 743216). A.S.H. is supported by an EMBO Long-term Postdoctoral Fellowship (ALTF 1095-2015) and the Alexander von Humboldt Foundation (FRA-1184902-HFST-P). We thank G. Tushev and the interns E. Seiffert, L. Hummer, and S. Hirshl for help with web visualization and G. Tushev for support with the NeuroBits software. We thank Dr. S. Tom Dieck for experimental support. The funders had no role in study design, data collection and analysis, decision to publish, or preparation of the manuscript.

AUTHOR CONTRIBUTIONS

Y.F., N.K., A.-S.H., T.T., and E.M.S. designed the study and wrote the manuscript. Y.F. performed mRNA and protein data analyses, steady-state model analyses, and simulations with input from T.T. N.K. performed mathematical analyses, computations, and simulations for the steady-state and dynamical evolution of mRNAs and proteins. A.S.H. provided experimental data and contributed to mRNA and protein data analyses. L.K. provided experimental immunostaining protein data and technical guidance for ImageJ. T.T. developed mRNA and protein visualization software and performed analyses on fractions of somatic and dendritic protein production based on Miller et al. experimental data. N.K., Y.F., A.-S.H., and E.M.S. contributed ideas to this analysis. F.S. contributed to the image analysis and simulation methods.

DECLARATION OF INTERESTS

The authors declare no competing interests.

Received: September 12, 2018
Revised: February 21, 2019
Accepted: June 22, 2019
Published: July 23, 2019

REFERENCES

Aakalu, G., Smith, W.B., Nguyen, N., Jiang, C., and Schuman, E.M. (2001). Dynamic visualization of local protein synthesis in hippocampal neurons. Neuron *30*, 489–502.

Akbalik, G., Langebeck-Jensen, K., Tushev, G., Sambandan, S., Rinne, J., Epstein, I., Cajigas, I., Vlatkovic, I., and Schuman, E.M. (2017). Visualization of newly synthesized neuronal RNA in vitro and in vivo using click-chemistry. RNA Biol. *14*, 20–28.

Banker, G., and Goslin, K. (1990). Culturing Nerve Cells (MIT Press).

Bingol, B., and Schuman, E.M. (2006). Activity-dependent dynamics and sequestration of proteasomes in dendritic spines. Nature *441*, 1144–1148.

Bressloff, P.C., and Earnshaw, B.A. (2007). Diffusion-trapping model of receptor trafficking in dendrites. Phys. Rev. E Stat. Nonlin. Soft Matter Phys. *75*, 041915.

Bressloff, P.C., and Newby, J.M. (2013). Stochastic models of intracellular transport. Rev. Mod. Phys. *85*, 135–196.

Buxbaum, A.R., Haimovich, G., and Singer, R.H. (2015). In the right place at the right time: visualizing and understanding mRNA localization. Nat. Rev. Mol. Cell Biol. *16*, 95–109.

Cajigas, I.J., Tushev, G., Will, T.J., tom Dieck, S., Fuerst, N., and Schuman, E.M. (2012). The local transcriptome in the synaptic neuropil revealed by deep sequencing and high-resolution imaging. Neuron *74*, 453–466.

Chen, C., Rainnie, D.G., Greene, R.W., and Tonegawa, S. (1994). Abnormal fear response and aggressive behavior in mutant mice deficient for alpha-calcium-calmodulin kinase II. Science *266*, 291–294.

Chen, X., Winters, C., Azzam, R., Li, X., Galbraith, J.A., Leapman, R.D., and Reese, T.S. (2008). Organization of the core structure of the postsynaptic density. Proc. Natl. Acad. Sci. USA *105*, 4453–4458.

Choquet, D., and Triller, A. (2013). The dynamic synapse. Neuron *80*, 691–703.

Cohen, L.D., Zuchman, R., Sorokina, O., Müller, A., Dieterich, D.C., Armstrong, J.D., Ziv, T., and Ziv, N.E. (2013). Metabolic turnover of synaptic proteins: kinetics, interdependencies and implications for synaptic maintenance. PLoS ONE *8*, e63191.

Czöndör, K., Mondin, M., Garcia, M., Heine, M., Frischknecht, R., Choquet, D., Sibarita, J.-B., and Thoumine, O.R. (2012). Unified quantitative model of AMPA receptor trafficking at synapses. Proc. Natl. Acad. Sci. USA *109*, 3522–3527.

Darzacq, X., Shav-Tal, Y., de Turris, V., Brody, Y., Shenoy, S.M., Phair, R.D., and Singer, R.H. (2007). In vivo dynamics of RNA polymerase II transcription. Nat. Struct. Mol. Biol. *14*, 796–806.

Davis, L., Burger, B., Banker, G.A., and Steward, O. (1990). Dendritic transport: quantitative analysis of the time course of somatodendritic transport of recently synthesized RNA. J. Neurosci. *10*, 3056–3068.

Dieterich, D.C., Hodas, J.J., Gouzer, G., Shadrin, I.Y., Ngo, J.T., Triller, A., Tirrell, D.A., and Schuman, E.M. (2010). *In situ* visualization and dynamics of newly synthesized proteins in rat hippocampal neurons. Nat. Neurosci. *13*, 897–905.

Dörrbaum, A.R., Kochen, L., Langer, J.D., and Schuman, E.M. (2018). Local and global influences on protein turnover in neurons and glia. eLife *7*, e34202.

Doyle, M., and Kiebler, M.A. (2011). Mechanisms of dendritic mRNA transport and its role in synaptic tagging. EMBO J. *30*, 3540–3552.

Dundr, M., Hoffmann-Rohrer, U., Hu, Q., Grummt, I., Rothblum, L.I., Phair, R.D., and Misteli, T. (2002). A kinetic framework for a mammalian RNA polymerase in vivo. Science *298*, 1623–1626.

Fiala, J.C., and Harris, K.M. (1999). Dendrite structure. In Dendrites, G. Stuart and M. Hausser, eds. (Royal Society Publishing), pp. 1–34.

Franker, M.A.M., and Hoogenraad, C.C. (2013). Microtubule-based transport - basic mechanisms, traffic rules and role in neurological pathogenesis. J. Cell Sci. *126*, 2319–2329.

Fusco, D., Accornero, N., Lavoie, B., Shenoy, S.M., Blanchard, J.-M., Singer, R.H., and Bertrand, E. (2003). Single mRNA molecules demonstrate probabilistic movement in living mammalian cells. Curr. Biol. *13*, 161–167.

Glock, C., Heumüller, M., and Schuman, E.M. (2017). mRNA transport and local translation in neurons. Curr. Opin. Neurobiol. *45*, 169–177.

Govindarajan, A., Israely, I., Huang, S.-Y., and Tonegawa, S. (2011). The dendritic branch is the preferred integrative unit for protein synthesis-dependent LTP. Neuron *69*, 132–146.

Hanus, C., and Schuman, E.M. (2013). Proteostasis in complex dendrites. Nat. Rev. Neurosci. *14*, 638–648.

Harris, K.M., and Weinberg, R.J. (2012). Ultrastructure of synapses in the mammalian brain. Cold Spring Harb. Perspect. Biol. *4*, a005587.

Hilgers, V., Perry, M.W., Hendrix, D., Stark, A., Levine, M., and Haley, B. (2011). Neural-specific elongation of 3′ UTRs during Drosophila development. Proc. Natl. Acad. Sci. USA *108*, 15864–15869.

Hirokawa, N., and Takemura, R. (2005). Molecular motors and mechanisms of directional transport in neurons. Nat. Rev. Neurosci. *6*, 201–214.

Hirokawa, N., Niwa, S., and Tanaka, Y. (2010). Molecular motors in neurons: transport mechanisms and roles in brain function, development, and disease. Neuron *68*, 610–638.

Holt, C.E., and Schuman, E.M. (2013). The central dogma decentralized: new perspectives on RNA function and local translation in neurons. Neuron *80*, 648–657.

Kaech, S., and Banker, G. (2006). Culturing hippocampal neurons. Nat. Protoc. *1*, 2406–2415.

Kanai, Y., Dohmae, N., and Hirokawa, N. (2004). Kinesin transports RNA: isolation and characterization of an RNA-transporting granule. Neuron *43*, 513–525.

Kennedy, M.B., Bennett, M.K., and Erondu, N.E. (1983). Biochemical and immunochemical evidence that the “major postsynaptic density protein” is a subunit of a calmodulin-dependent protein kinase. Proc. Natl. Acad. Sci. USA *80*, 7357–7361.

Khan, S., Reese, T.S., Rajpoot, N., and Shabbir, A. (2012). Spatiotemporal maps of CaMKII in dendritic spines. J. Comput. Neurosci. *33*, 123–139.

Koleske, A.J. (2013). Molecular mechanisms of dendrite stability. Nat. Rev. Neurosci. *14*, 536–550.

Lu, H.E., MacGillavry, H.D., Frost, N.A., and Blanpied, T.A. (2014). Multiple spatial and kinetic subpopulations of CaMKII in spines and dendrites as resolved by single-molecule tracking PALM. J. Neurosci. *34*, 7600–7610.

Magee, J.C. (1998). Dendritic hyperpolarization-activated currents modify the integrative properties of hippocampal CA1 pyramidal neurons. J. Neurosci. *18*, 7613–7624.

Malenka, R.C., Kauer, J.A., Perkel, D.J., Mauk, M.D., Kelly, P.T., Nicoll, R.A., and Waxham, M.N. (1989). An essential role for postsynaptic calmodulin and protein kinase activity in long-term potentiation. Nature *340*, 554–557.

Mayford, M., Baranes, D., Podsypanina, K., and Kandel, E.R. (1996). The 3′-untranslated region of CaMKII α is a cis-acting signal for the localization and translation of mRNA in dendrites. Proc. Natl. Acad. Sci. USA *93*, 13250–13255.

Metzler, R., and Klafter, J. (2000). The random walk’s guide to anomalous diffusion: a fractional dynamics approach. Phys. Rep. *339*, 1–77.

Miller, S., Yasuda, M., Coats, J.K., Jones, Y., Martone, M.E., and Mayford, M. (2002). Disruption of dendritic translation of CaMKIIalpha impairs stabilization of synaptic plasticity and memory consolidation. Neuron *36*, 507–519.

Park, H.Y., Lim, H., Yoon, Y.J., Follenzi, A., Nwokafor, C., Lopez-Jones, M., Meng, X., and Singer, R.H. (2014). Visualization of dynamics of single endogenous mRNA labeled in live mouse. Science *343*, 422–424.

Pfeiffer, T., Poll, S., Bancelin, S., Angibaud, J., Inavalli, V.K., Keppler, K., Mittag, M., Fuhrmann, M., and Nägerl, U.V. (2018). Chronic 2P-STED imaging reveals high turnover of dendritic spines in the hippocampus in vivo. eLife *7*, e34700.

Ranft, J., Almeida, L.G., Rodriguez, P.C., Triller, A., and Hakim, V. (2017). An aggregation-removal model for the formation and size determination of post-synaptic scaffold domains. PLoS Comput. Biol. *13*, e1005516.

Rangaraju, V., Lauterbach, M., and Schuman, E.M. (2019). Spatially stable mitochondrial compartments fuel local translation during plasticity. Cell *176*, 73–84.e15.

Santamaria, F., Wils, S., De Schutter, E., and Augustine, G.J. (2006). Anomalous diffusion in Purkinje cell dendrites caused by spines. Neuron *52*, 635–648.

Schindelin, J., Arganda-Carreras, I., Frise, E., Kaynig, V., Longair, M., Pietzsch, T., Preibisch, S., Rueden, C., Saalfeld, S., Schmid, B., et al. (2012). Fiji: an open-source platform for biological-image analysis. Nat. Methods *9*, 676–682.

Schwanhäusser, B., Busse, D., Li, N., Dittmar, G., Schuchhardt, J., Wolf, J., Chen, W., and Selbach, M. (2011). Global quantification of mammalian gene expression control. Nature *473*, 337–342.

Shen, K., and Meyer, T. (1999). Dynamic control of CaMKII translocation and localization in hippocampal neurons by NMDA receptor stimulation. Science *284*, 162–166.

Silva, A.J., Paylor, R., Wehner, J.M., and Tonegawa, S. (1992). Impaired spatial learning in α-calcium-calmodulin kinase II mutant mice. Science *257*, 206–211.

Smith, W.B., Starck, S.R., Roberts, R.W., and Schuman, E.M. (2005). Dopaminergic stimulation of local protein synthesis enhances surface expression of GluR1 and synaptic transmission in hippocampal neurons. Neuron *45*, 765–779.

Sutton, M.A., and Schuman, E.M. (2006). Dendritic protein synthesis, synaptic plasticity, and memory. Cell *127*, 49–58.

Taylor, A.M., Dieterich, D.C., Ito, H.T., Kim, S.A., and Schuman, E.M. (2010). Microfluidic local perfusion chambers for the visualization and manipulation of synapses. Neuron *66*, 57–68.

Tian, B., and Manley, J.L. (2017). Alternative polyadenylation of mRNA precursors. Nat. Rev. Mol. Cell Biol. *18*, 18–30.

Triesch, J., Vo, A.D., and Hafner, A.-S. (2018). Competition for synaptic building blocks shapes synaptic plasticity. eLife *7*, e37836.

Tushev, G., Glock, C., Heumüller, M., Biever, A., Jovanovic, M., and Schuman, E.M. (2018). Alternative 3′ UTRs modify the localization, regulatory potential, stability, and plasticity of mRNAs in neuronal compartments. Neuron *98*, 495–511.e6.

Williams, A.H., O’Donnell, C., Sejnowski, T.J., and O’Leary, T. (2016). Dendritic trafficking faces physiologically critical speed-precision tradeoffs. eLife *5*, 1–25.

Wu, B., Eliscovich, C., Yoon, Y.J., and Singer, R.H. (2016). Translation dynamics of single mRNAs in live cells and neurons. Science *352*, 1430–1435.

Yang, E., van Nimwegen, E., Zavolan, M., Rajewsky, N., Schroeder, M., Magnasco, M., and Darnell, J.E., Jr. (2003). Decay rates of human mRNAs: correlation with functional characteristics and sequence attributes. Genome Res. *13*, 1863–1872.

Yoon, Y.J., Wu, B., Buxbaum, A.R., Das, S., Tsai, A., English, B.P., Grimm, J.B., Lavis, L.D., and Singer, R.H. (2016). Glutamate-induced RNA localization and translation in neurons. Proc. Natl. Acad. Sci. USA *113*, E6877–E6886.

Zalfa, F., Giorgi, M., Primerano, B., Moro, A., Di Penta, A., Reis, S., Oostra, B., and Bagni, C. (2003). The fragile X syndrome protein FMRP associates with BC1 RNA and regulates the translation of specific mRNAs at synapses. Cell *112*, 317–327.

Zhang, Y.-P., Holbro, N., and Oertner, T.G. (2008). Optical induction of plasticity at single synapses reveals input-specific accumulation of alphaCaMKII. Proc. Natl. Acad. Sci. USA *105*, 12039–12044.

Zhao, C., Teng, E.M., Summers, R.G., Jr., Ming, G.L., and Gage, F.H. (2006). Distinct morphological stages of dentate granule neuron maturation in the adult mouse hippocampus. J. Neurosci. *26*, 3–11.

STAR★METHODS

KEY RESOURCES TABLE

REAGENT or RESOURCE	SOURCE	IDENTIFIER
Antibodies		
Rabbit polyclonal anti-CamK2α	Millipore	RRID:04-1079
Guinea pig polyclonal anti-MAP2	Synaptic Systems	RRID:188004
Goat anti-Guinea pig Alexa Fluor 488	Invitrogen	RRID:A11073
Goat anti-Rabbit Alexa Fluor 594	Invitrogen	RRID:A11037
DAPI	Sigma-Aldrich	RRID:28718-90-3
Critical Commercial Assays		
Quantigene ViewRNA ISH Cell Assay	Thermo Fisher Scientific	RRID:QVC0001
Experimental Model: Cell Line		
Rat hippocampal cultured neurons from P0-1	Charles Rivers	RRID: RGD_734476
Experimental Model: Organism/Strain		
Rattus norvegicus, Sprague-Dawley	Charles Rivers	RRID: RGD_734476
Chemicals, Peptides, and Recombinant Proteins		
Papain	Sigma-Aldrich	RRID:P-3125
Neurobasal-A	Life Technologies	RRID:10888022
B27	GIBCO	RRID:17504044
GlutaMax	GIBCO	RRID:35050038
Software and Algorithms		
Fiji	Schindelin et al., 2012	https://imagej.net/Welcome
MATLAB	MathWorks	https://www.mathworks.com
Mathematica	Wolfram Research	http://www.wolfram.com
NeuroBits	Tushev et al., 2018	https://github.molgen.mpg.de/MPIBR/NeuroBits
mRNA and protein steady states and dynamics visualization	This paper	http://www.tchumatchenko.de/Visualisation.html
Data and Software Availability		
Raw image data	This paper	http://www.tchumatchenko.de/Visualisation.html
Code	This paper	http://www.tchumatchenko.de/Visualisation.html
Other		
LSM880	Zeiss	https://www.zeiss.de/mikroskopie/produkte/confocal-microscopes/lsm-880.html

LEAD CONTACT AND MATERIALS AVAILABILITY

Further requests for resources should be directed to and will be fulfilled by the Lead Contact, Tatjana Tchumatchenko (tatjana.tchumatchenko@brain.mpg.de).

EXPERIMENTAL MODEL AND SUBJECT DETAILS

Hippocampal neuron preparation

Dissociated hippocampal neuron cultures were prepared from postnatal day 0 to 1 rat pups of either sex (Sprague-Dawley strain; Charles River Laboratories). We dissected hippocampi, dissociated them with papain (Sigma) and plated them at a density of 40–30 × 10^3 cells/cm^2 onto poly(d-lysine)-coated (BD Biosciences) glass-bottom Petri dishes (MatTek). Hippocampal neurons were maintained, fed weekly with neuronal growth medium and allowed to mature in a humidified atmosphere at 37°C and 5% CO_2 in growth medium (Neurobasal-A supplemented with B27 and GlutaMAX-I, Life Technologies) for >18 d *in vitro* to ensure synapse maturation. All experiments complied with national animal care guidelines and the guidelines issued by the Max Planck Society, and were approved by local authorities. The procedures involving animal treatment and care were conducted in conformity with the institutional guidelines that are in compliance with national and international laws and policies (DIRECTIVE 2010/63/EU; German animal welfare law; FELASA guidelines). The animals were euthanized according to annex 2 of §2 Abs. 2 Tierschutz-Versuchstier-Verordnung. Let us note, that this protocol is consistent with previously published protocols (Aakalu et al., 2001; Banker and Goslin, 1990).

METHOD DETAILS

Methods for *in vitro* measurements of CaMKIIα mRNA and protein

RNA in situ *hybridization and immunostaining*

All subsequent steps were performed at room temperature, if not stated otherwise. Bottom glass dishes with attached neurons (DIV 18-21) were washed and fixed once in room temperature phosphate-buffered saline (PBS) containing 2 mg calcium chloride and 2 mg magnesium chloride before being fixed in paraformaldehyde 4% in lysine phosphate buffer (pH = 7.4) containing 2.5% of sucrose. Cells were then permeabilized for 10 min in PBS containing 0.5% Triton X-100 (Sigma). *In situ* hybridization was performed using the QuantiGene (QG) ViewRNA kit from Panomics as previously described (Taylor et al., 2010) with the following modifications. The Proteinase K treatment was omitted in order to preserve the integrity of the dendrites. After completion of *in situ* hybridizations, cells were washed with PBS and subsequently processed for immunofluorescence of MAP2. Cells were incubated in blocking buffer (4% goat serum in PBS) for 30 min and then incubated for 1–2 h at room temperature with primary antibodies in blocking buffer. We used the following antibodies: guinea pig anti-MAP2 (Synaptic Systems, 1:2000) and rabbit CaMKIIα (Millipore, 1:2000). Secondary antibodies were applied in blocking buffer for 1 h at room temperature, nuclei were stained for 1 min in PBS with DAPI (Sigma-Aldrich, 1:1000). Preparation of neurons for protein immunostaining followed the same procedure as for mRNA, described above but including anti-CamKII antibody and anti-MAP2 antibody.

Image acquisition

Hippocampal neurons were imaged using Zeiss LSM780/880 confocal microscopes and 63X (high-resolution *in situ* hybridization samples) and 40X (CaMKIIα protein, immunofluorscence samples) oil objectives (NA 1.4). Z stacks spanning the entire volume of neurons were obtained and channels were separated and collapsed to a sum intensity projection in ImageJ.

Image analysis for mRNA measurements

Images were analyzed using a custom-built MATLAB assembly of widgets called NeuroBits to record the distance of all puncta from each neuron's soma. The code and instruction manual for NeuroBits is freely available for download online https://github.molgen.mpg.de/MPIBR/NeuroBits. Briefly, using user inputs, neurons were segmented into their soma and dendritic segments. Each segment was then connected in a "dendritic tree," or a representation of how the primary branches (segments originating directly from the soma) were connected to secondary, tertiary, and subsequent higher-order branches. Using modifiable parameters for the minimum puncta size and intensity, NeuroBits then automatically detected every mRNA puncta on each of the branches, their specific location on a branch and their distance from the soma. In our analysis of the 21 neurons, mRNA puncta on 403 dendrites were analyzed. We found 483 puncta located on the considered dendritic segments that were at least 100 μm long. Finally, using the minimum dendritic branch length of 100 μm, the distribution of all mRNA puncta with that length was evaluated. For more detailed instructions about how to use NeuroBits, see its README file.

Image analysis for protein measurements

20 neurons immmunostained for endogenous CaMKIIα protein were analyzed. The fluorescence intensity signal from the immunostainings were obtained using the open-source image processing package Fiji, while the data analysis was performed in MATLAB R2017b (MathWorks). For each neuron, the soma and dendrites were segmented. To do so, each image stack was separated into three channels representing the dendritic arbor, the nucleus, and the CaMKIIα signal. The dendritic arbor and soma of each neuron was then traced with segmented lines of a constant width. Using a sum intensity projection of the CaMKIIα channel we measured the fluorescence intensity of CaMKIIα as a function of dendritic distance. A threshold mask of each neuron was made by an experienced experimentalist to determined the area of the dendritic segments. Finally, we used this mask to normalize CaMKIIα fluorescence intensity signal as a function of dendritic distance by the area. A batch-script for ImageJ was written to facilitate the measurement and normalization process. Plots of all the fluorescence intensity signals as well as the average signal and confidence intervals were generated in MATLAB.

Deriving the spatiotemporal mRNA dynamics

To solve Equation 1, we first transform it into the form of a diffusion equation by introducing an auxiliary function $\overline{R}$ which we define as

$$\overline{R}(x,t) = R(x,t)e^{\eta_R t - \mu_R x}, \qquad \text{(Equation 6)}$$

whereby $\eta_R = k_R + \nu_R^2/(4D_R)$ and $\mu_R = \nu_R/(2D_R)$. The equation governing the dynamics of $\overline{R}$ now reads

$$\frac{\partial \overline{R}(x,t)}{\partial t} = D_R \frac{\partial^2 \overline{R}(x,t)}{\partial x^2}. \qquad \text{(Equation 7)}$$

To obtain the solution R of Equation 1 we first determine the solution $\overline{R}$ of Equation 7 and apply Equation 6. To find $\overline{R}$ we solve the Laplace transformed Equation 7 and transform the corresponding solution back into the time domain. The Laplace transformed Equation 7 reads

$$s\tilde{R}(x,s) = D_R \frac{\partial^2 \tilde{R}(x,s)}{\partial x^2}, \tag{Equation 8}$$

where $\tilde{R}(x,s)$ is the Laplace transform of $\overline{R}(x,t)$. The Laplace transform of $(\partial/\partial t)\,\overline{R}(x,t)$ is $s\tilde{R}(x,s) - \overline{R}(x,0)$. Since we consider only mRNA that are produced after $t = 0$, we obtain $\overline{R}(x,0) = 0$. The solution of Equation 8 has the form

$$\tilde{R}(x,s) = C_1 e^{-x\sqrt{sD_R^{-1}}} + C_2 e^{x\sqrt{sD_R^{-1}}}, \tag{Equation 9}$$

whereby C_1 and C_2 are constants that we need to determine. Since it is not biologically plausible that the number of mRNAs increases to infinity as a function of distance from the soma, we conclude that $C_2 = 0$. To obtain the constant C_1 we use the equation $R(0,t) = \beta_R/\gamma_R\left(1 - e^{-\gamma_R t}\right)$ that describes how the balance between production and removal of mRNA evolves on the boundary between soma and dendrites. Here, β_R is the average transcription rate, γ_R denotes mRNA removal rate which includes mRNA diffusion and active transport away from the soma as well as mRNA degradation. Later in this section we derive $\gamma_R = k_R/\lambda_R$ where $\lambda_R = \left(\sqrt{\nu_R^2 + 4D_R k_R} - \nu_R\right)\Big/(2D_R)$. The Laplace transform applied to $\overline{R}(0,t)$ leads to the relation

$$\tilde{R}(0,s) = \frac{\beta_R}{\gamma_R}\left(-\frac{1}{s - \eta_R + \gamma_R} + \frac{1}{s - \eta_R}\right).$$

Using this expression we determine the constant C_1 and obtain the solution $\tilde{R}$ of Equation 8

$$\tilde{R}(x,s) = \frac{\beta_R}{\gamma_R}\left(-\frac{1}{s - \eta_R + \gamma_R} + \frac{1}{s - \eta_R}\right)e^{-\frac{x\sqrt{s}}{\sqrt{D_R}}}. \tag{Equation 10}$$

Next, we calculate the inverse Laplace transform of $\tilde{R}$, obtain the solution $\overline{R}$ of Equation 7 and then the solution R of Equation 1

$$R(x,t) = \frac{\beta_R e^{\mu_R x}}{2\gamma_R}\left(-e^{-\gamma_R t}\mathcal{E}_{erfc}\left(\frac{x}{2\sqrt{D_R}}, \sqrt{\eta_R - \gamma_R}, \frac{1}{\sqrt{t}}\right) + \mathcal{E}_{erfc}\left(\frac{x}{2\sqrt{D_R}}, \sqrt{\eta_R}, \frac{1}{\sqrt{t}}\right)\right), \tag{Equation 11}$$

whereby

$$\mathcal{E}_{erfc}(\alpha,\beta,\gamma) = e^{2\alpha\beta}\mathrm{erfc}\left(\alpha\gamma + \beta\gamma^{-1}\right) + e^{-2\alpha\beta}\mathrm{erfc}\left(\alpha\gamma - \beta\gamma^{-1}\right). \tag{Equation 12}$$

This solution has the following properties. First, at time zero no mRNA are present, $R(x,0) = 0$, which represents the start of transcription or the labeling of newly transcribed mRNAs. Second, this function can assume only real values even though the argument $\sqrt{\eta_R - \gamma_R}$ of $\mathcal{E}_{erfc}$ can be complex. We show this property in the STAR Method section "Functions $\mathcal{E}_{erf}$ and $\mathcal{E}_{erfc}$, related to Equations 11, 4, and 31."

The solution Equation 11 of Equation 1 approaches the steady state given by

$$R_{ss}^{den}(x) = \frac{\beta_R}{\gamma_R}\cdot\exp(-\lambda_R x). \tag{Equation 13}$$

Since only the somatic production and degradation rates determine the number of mRNAs along the dendrite we assume that the equation $\int_0^\infty R_{ss}^{den}(x)dx = \beta_R/k_R$ holds. This equation leads to the relation $\gamma_R = k_R/\lambda_R$.

Deriving the spatiotemporal protein dynamics

To solve Equation 3, we take steps similar to those above and first transform Equation 3 into the form of a diffusion equation by introducing an auxiliary function $\overline{P}$ which we define as

$$\overline{P}(x,t) = e^{\eta_P t - \mu_P x}P(x,t), \tag{Equation 14}$$

whereby $\eta_P = k_P + \nu_P^2/(4D_P)$, $\mu_P = \nu_P/(2D_P)$. The equation governing the dynamics of $\overline{P}$ now reads

$$\frac{\partial \overline{P}(x,t)}{\partial t} = D_P \frac{\partial^2 \overline{P}(x,t)}{\partial x^2} + \beta_P R_{ss}^{den}(x)e^{\eta_P t - \mu_P x}. \tag{Equation 15}$$

In order to find P, we first obtain the solution $\overline{P}$ of Equation 15 and then apply Equation 14. To find $\overline{P}(x,t)$ we transform Equation 15 into the Laplace domain, obtain a solution and then transform it back into the time domain. The Laplace transformed Equation 15 reads

$$s\tilde{P}(x,s) = D_P \frac{\partial^2 \tilde{P}(x,s)}{\partial x^2} + \frac{\beta_P \beta_R \lambda_R}{k_R}\frac{e^{-(\lambda_R + \mu_P)x}}{s - \eta_P}. \tag{Equation 16}$$

$\tilde{P}(x,s)$ is the Laplace transform of $\overline{P}(x,t)$. The balance between production, degradation, and transport on the boundary between soma and dendrites evolves according to $P(0,t) = (\beta_P\beta_R/\gamma_P\gamma_R)(1-e^{-\gamma_P t})$. Here γ_P represents protein removal rate analogously to the mRNA parameter γ_R. Later in this section we show that $\gamma_P = k_P(D_P\lambda_R^2 + \nu_P\lambda_R - k_P)/(D_P\lambda_R\lambda_P + \nu_P\lambda_P - k_P)$, where $\lambda_P = \left(\sqrt{\nu_P^2+4D_Pk_P}-\nu_P\right)\Big/(2D_P)$. The solution of Equation 16 takes the form

$$\tilde{P}(x,s) = \frac{\beta_P\beta_R\lambda_R}{k_R\left(k_P - D_P\lambda_R^2 - \lambda_R\nu_P\right)} \times \left(\frac{e^{-(\lambda_R+\mu_P)x}}{s-\eta_P} - \frac{e^{-(\lambda_R+\mu_P)x}}{s-D_P(\lambda_R+\mu_P)^2} - \frac{\lambda_P(D_P\lambda_R+\nu_P)e^{-\frac{x}{\sqrt{D_P}}\sqrt{s}}}{k_P(s-\eta_P)} + \frac{(D_P\lambda_R\lambda_P+\nu_P\lambda_P-k_P)e^{-\frac{x}{\sqrt{D_P}}\sqrt{s}}}{k_P(s-\eta_P+\gamma_P)} + \frac{e^{-\frac{x}{\sqrt{D_P}}\sqrt{s}}}{s-D_P(\lambda_R+\mu_P)^2}\right). \tag{Equation 17}$$

Next, we apply the inverse Laplace transform to Equation 17 and use Equation 14. We obtain

$$P(x,t) = \frac{\beta_P\beta_R\lambda_R e^{\mu_P x}}{k_R\left(k_P - D_P\lambda_R^2 - \lambda_R\nu_P\right)} \times \left(e^{-(\lambda_R+\mu_P)x}\left(1-e^{\left(D_P(\lambda_R+\mu_P)^2-\eta_P\right)t}\right) + \frac{-\lambda_P(D_P\lambda_R+\nu_P)\mathcal{E}_{erfc}\left(\frac{x}{2\sqrt{D_P}},\sqrt{\eta_P},\frac{1}{\sqrt{t}}\right) + (D_P\lambda_R\lambda_P+\nu_P\lambda_P-k_P)e^{-\gamma_P t}\mathcal{E}_{erfc}\left(\frac{x}{2\sqrt{D_P}},\sqrt{\eta_P-\gamma_P},\frac{1}{\sqrt{t}}\right)}{2k_P} + \frac{e^{\left(D_P(\lambda_R+\mu_P)^2-\eta_P\right)t}\mathcal{E}_{erfc}\left(\frac{x}{2\sqrt{D_P}},\sqrt{D_P}(\lambda_R+\mu_P),\frac{1}{\sqrt{t}}\right)}{2}\right) \tag{Equation 18}$$

whereby

$$\mathcal{E}_{erfc}(\alpha,\beta,\gamma) = e^{2\alpha\beta}\mathrm{erfc}\left(\alpha\gamma+\beta\gamma^{-1}\right) + e^{-2\alpha\beta}\mathrm{erfc}\left(\alpha\gamma-\beta\gamma^{-1}\right). \tag{Equation 19}$$

This solution has the following properties. First, at time zero no protein are present, $P(x,0) = 0$, which represents the start of translation or the start of the labeling of newly synthesized proteins. Second, this function can assume only real values even though the arguments of $\mathcal{E}_{erfc}(\alpha,\beta,\gamma)$ can be complex. We show this property in the STAR Method section "Functions $\mathcal{E}_{erf}$ and $\mathcal{E}_{erfc}$, related to Equations 11, 4, and 31." The steady state of Equation 3 takes the form

$$P_{ss}^{den}(x) = -\frac{\beta_P\beta_R\lambda_R}{k_R\left(D_P\lambda_R^2+\nu_P\lambda_R-k_P\right)}\left(e^{-\lambda_R x}-e^{-\lambda_P x}\right) + \frac{\beta_P\beta_R\lambda_R}{k_R\gamma_P}e^{-\lambda_P x}.$$

Since the total number of the proteins is determined only by the production and degradation rates and is not affected by the movement parameters it satisfies $\int_0^\infty P_{ss}^{den}(x)dx = \beta_R\beta_P/(k_R k_P)$. This equation leads to the equation describing the removal rate γ_P which we used to derive Equation 4. The steady state P_{ss}^{den} now takes the form given by Equation 4.

Deriving the response to translational bursts

Here, we derive the dendritic protein response to a brief, local translational burst of the form $X(x) \cdot T(t)$. The spatial structure of the burst is described by $X(x)$ and its temporal structure by $T(t)$. $X(x)$ is a Gaussian centered at x_0 which has a width σ and the amplitude β_b. β_b represents the translational rate during the burst.

$$X(x) = \beta_b \exp\left(-(x-x_0)^2\Big/\sigma\right). \tag{Equation 20}$$

$T(t)$ has a finite on and off kinetics and its shape is described by a combination of exponentials of the form

$$T(t) = \Theta(t-t_0)(t-t_0)(a_1\exp(-a_2(t-t_0)) - b_1\exp(-b_2(t-t_0)))/T_{Max}, \tag{Equation 21}$$

where $\Theta(t-t_0)=1$ for $t \geq t_0$ and 0 for $t<t_0$. The parameters a_2 and b_2 are the on and off time constants and a_1, b_1 their corresponding weights. Normalization by T_{Max} ensures that $T(t)$ has a maximal value of one. To mimic the experimentally recorded duration of a translational burst of approximately 10-20 mins (Wu et al., 2016) we set $a_1 = 1$, $a_2 = (5 \cdot 60)^{-1}$ 1/s, $b_1 = 0.1$, $b_2 = (5 \cdot 60)^{-1}$ 1/s (Figure 6). Protein dynamics in response to a translational burst is described by

$$\frac{\partial P(x,t)}{\partial t} = D_P\frac{\partial P(x,t)}{\partial x^2} - \nu_P\frac{\partial P(x,t)}{\partial x} - k_P P(x,t) + X(x)T(t). \tag{Equation 22}$$

To solve Equation 22, we first transform it into the form of a diffusion equation by introducing the auxiliary function $\overline{P}$ which we define as

$$\overline{P}(x,t) = e^{\eta_P t - \mu_P x} P(x,t) \tag{Equation 23}$$

whereby $\eta_P = k_P + \nu_P^2/(4D_P)$, $\mu_P = \nu_P/(2D_P)$. The second variable substitution rescales the distance

$$x = y\sqrt{D_P} \tag{Equation 24}$$

and leads to the following relation $\overline{\overline{P}}(y,t) = \overline{\overline{P}}(x/\sqrt{D_P},t) = \overline{P}(x,t)$. The rescaled dynamics for the y-dependent function $\overline{\overline{P}}$ reads

$$\overline{\overline{P}}_t(y,t) - \overline{\overline{P}}_{yy}(y,t) = X\left(y\sqrt{D_P}\right) T(t) e^{\eta_P t - \mu_P y\sqrt{D_P}}. \tag{Equation 25}$$

The solution of Equation 25 is

$$\overline{\overline{P}}(y,t) = \frac{\beta_b}{2\sqrt{\pi}} \int_0^t \frac{T(s)e^{\eta_P s} ds}{(t-s)^{1/2}} \int_{-\infty}^{\infty} e^{-\frac{(y-z)^2}{4(t-s)} - \mu_P z\sqrt{D_P} - \frac{\left(z\sqrt{D_P} - x_0\right)^2}{\sigma}} dz. \tag{Equation 26}$$

To derive Equation 26, we use the fundamental solution of the diffusion equation presented in the STAR Methods section ”Fundamental solution of the diffusion equation, related to Equation 22.” Solving the double integral takes several steps. First, we rewrite the argument of the exponential function as a quadratic polynomial with respect to the variable z

$$\frac{(y-z)^2}{4(t-s)} + \mu_P z\sqrt{D_P} + \frac{\left(z\sqrt{D_P} - x_0\right)^2}{\sigma} = A\left(z + \frac{B}{A}\right)^2 + C - \frac{B^2}{A} \tag{Equation 27}$$

where

$$A = \frac{\sigma + 4(t-s)D_P}{4\sigma(t-s)}, \quad B = \frac{2(t-s)\sqrt{D_P}(\sigma\mu_P - 2x_0) - y\sigma}{4\sigma(t-s)}, \quad C = \frac{\sigma y^2 + 4x_0^2(t-s)}{4\sigma(t-s)}. \tag{Equation 28}$$

This allows us to solve the inner integral which results in

$$\int_{-\infty}^{\infty} e^{-\frac{(y-z)^2}{4(t-s)} - \mu_P z\sqrt{D_P} - \frac{\left(z\sqrt{D_P} - x_0\right)^2}{\sigma}} dz = \frac{\sqrt{\pi} e^{\frac{B^2}{A} - C}}{\sqrt{A}}. \tag{Equation 29}$$

From $\overline{\overline{P}}(y,t)$ we now obtain $P(x,t)$ by applying Equations 24 and 23.

$$P(x,t) = \beta_b\sqrt{\sigma} e^{\frac{\sigma\mu_P^2}{4} + \mu_P(x - x_0) - \eta_P t} \int_0^t \frac{T(s) e^{\eta_P s - \frac{(\sigma\mu_P + 2(x - x_0))^2}{4(\sigma + 4D_P(t-s))}}}{\sqrt{\sigma + 4(t-s)D_P}} ds. \tag{Equation 30}$$

The closed-form solution of this integral is

$$\begin{aligned} P(x,t) = {} & \frac{\beta_b\sqrt{\sigma} e^{\frac{\sigma\mu_P^2}{2} + \frac{\sigma k_P}{4D_P} + \mu_P(x - x_0)}}{16 T_{Max} D_P^2} \cdot \left(a_1 e^{-a_2\left(t - t_0 + \frac{\sigma}{4D_P}\right)} \left(\mathcal{I}_{-\frac{1}{2}}(a,b,\mathcal{A}_1,\mathcal{B})(4D_P(t - t_0) + \sigma) - \mathcal{I}_{\frac{1}{2}}(a,b,\mathcal{A}_1,\mathcal{B})\right) \right. \\ & \left. + b_1 e^{-b_2\left(t - t_0 + \frac{\sigma}{4D_P}\right)} \left(\mathcal{I}_{\frac{1}{2}}(a,b,\mathcal{A}_2,\mathcal{B}) - (4D_P(t - t_0) + \sigma)\mathcal{I}_{-\frac{1}{2}}(a,b,\mathcal{A}_2,\mathcal{B})\right) \right) \end{aligned} \tag{Equation 31}$$

with $a = \sigma$, $b = \sigma + 4D_P(t - t_0)$, $\mathcal{A}_1 = (\eta_P - a_2)/(4D_P)$, $\mathcal{A}_2 = (\eta_P - b_2)/(4D_P)$ and $\mathcal{B} = (\sigma\mu_P + 2(x - x_0))^2/4$. Whereby

$$\mathcal{I}_{-\frac{1}{2}}(a,b,\mathcal{A},\mathcal{B}) = \frac{1}{2}\sqrt{\frac{\pi}{A}}\left(\mathcal{E}_{erf}\left(\sqrt{A},\sqrt{B},\sqrt{b}\right) - \mathcal{E}_{erf}\left(\sqrt{A},\sqrt{B},\sqrt{a}\right)\right),$$

$$\begin{aligned} \mathcal{I}_{\frac{1}{2}}(a,b,\mathcal{A},\mathcal{B}) = {} & -\frac{1}{A}\left(b^{\frac{1}{2}} e^{-Ab - Bb^{-1}} - a^{\frac{1}{2}} e^{-Aa - Ba^{-1}}\right) + \frac{1}{4A}\frac{\sqrt{\pi}}{\sqrt{A}}\left(\mathcal{E}_{erf}\left(\sqrt{A},\sqrt{B},\sqrt{b}\right) - \mathcal{E}_{erf}\left(\sqrt{A},\sqrt{B},\sqrt{a}\right)\right) \\ & + \frac{\sqrt{B\pi}}{2A}\left(\mathcal{E}_{erf}\left(\sqrt{B},\sqrt{A},\sqrt{a^{-1}}\right) - \mathcal{E}_{erf}\left(\sqrt{B},\sqrt{A},\sqrt{b^{-1}}\right)\right) \end{aligned}$$

and

$$\mathcal{E}_{erf}(\alpha,\beta,\gamma) = e^{2\alpha\beta}\mathrm{erf}\left(\alpha\gamma + \beta\gamma^{-1}\right) + e^{-2\alpha\beta}\mathrm{erf}\left(\alpha\gamma - \beta\gamma^{-1}\right).$$

Mathematical details on functions $\mathcal{E}_{erf}$ and $\mathcal{E}_{erfc}$

The mRNA and protein dynamics involve the functions

$$\mathcal{E}_{erf}(\alpha,\beta,\gamma) = e^{2\alpha\beta}\mathrm{erf}\left(\alpha\gamma+\beta\gamma^{-1}\right)+e^{-2\alpha\beta}\mathrm{erf}\left(\alpha\gamma-\beta\gamma^{-1}\right) \qquad \text{(Equation 32)}$$

$$\mathcal{E}_{erfc}(\alpha,\beta,\gamma) = e^{2\alpha\beta}\mathrm{erfc}\left(\alpha\gamma+\beta\gamma^{-1}\right)+e^{-2\alpha\beta}\mathrm{erfc}\left(\alpha\gamma-\beta\gamma^{-1}\right). \qquad \text{(Equation 33)}$$

Since β can be the root of a negative number it can take on imaginary values. For example, in Equation 18 $\beta=\sqrt{\eta_P-\gamma_P}$ is imaginary if $\eta_P<\gamma_P$. We show that both $\mathcal{E}_{erf}(\alpha,ib,\gamma)$ and $\mathcal{E}_{erfc}(\alpha,ib,\gamma)$ with a real b are given by

$$\mathcal{E}_{erf}(\alpha,ib,\gamma) = 2\mathcal{R}e\left(e^{i2\alpha b}\mathrm{erf}\left(\alpha\gamma+ib\gamma^{-1}\right)\right), \quad \mathcal{E}_{erfc}(\alpha,ib,\gamma)=2\mathcal{R}e\left(e^{i2\alpha b}\mathrm{erfc}\left(\alpha\gamma+ib\gamma^{-1}\right)\right). \qquad \text{(Equation 34)}$$

This property emerges from the observation that $\mathrm{erf}(\overline{z}) = \overline{\mathrm{erf}(z)}$. By reformulating $\mathcal{E}_{erf}(\alpha,ib,\gamma)$ using $z=\alpha\gamma+ib\gamma^{-1}$ and $v=2\alpha b$ we obtain

$$\mathcal{E}_{erf}(\alpha,ib,\gamma) = e^{iv}\mathrm{erf}(z)+e^{-iv}\mathrm{erf}(\overline{z})=e^{iv}\mathrm{erf}(z)+\overline{e^{iv}\mathrm{erf}(z)}=2\mathcal{R}e\left(e^{iv}\mathrm{erf}(z)\right). \qquad \text{(Equation 35)}$$

The second equation in (34) can be obtained analogously, since $\mathrm{erfc}(z)=1-\mathrm{erf}(z)$ and therefore, $\mathrm{erfc}(\overline{z}) = \overline{\mathrm{erfc}(z)}$.

Mathematical details on integrals $\int v^{\eta}e^{-Av-Bv^{-1}}dv$

Solving Equations 1, 3, and 22 requires calculating integrals of the form

$$\mathcal{I}_{\eta}(a,b,A,B)=\int_a^b v^{\eta}e^{-Av-Bv^{-1}}dv$$

where $\eta\in\{-3/2,-1/2,1/2\}$. We will express the result using the function $\mathcal{E}_{erf}$ or $\mathcal{E}_{erfc}$.

1. We first compute the integral $\mathcal{I}_{-\frac{1}{2}}(a,b,A,B)$. To this end, we split $\mathcal{I}_{-\frac{1}{2}}(a,b,A,B)$ into two integrals

$$\mathcal{I}_{-\frac{1}{2}}=\frac{1}{\sqrt{A}}\left(\frac{1}{2}\int_a^b\left(A^{\frac{1}{2}}v^{-\frac{1}{2}}+B^{\frac{1}{2}}v^{-\frac{3}{2}}\right)e^{-Av-Bv^{-1}}dv+\frac{1}{2}\int_a^b\left(A^{\frac{1}{2}}v^{-\frac{1}{2}}-B^{\frac{1}{2}}v^{-\frac{3}{2}}\right)e^{-Av-Bv^{-1}}dv\right). \qquad \text{(Equation 36)}$$

To compute the first integral we substitute $\mu=A^{1/2}v^{1/2}-B^{1/2}v^{-1/2}$ and obtain

$$\frac{1}{2}\int_a^b\left(A^{\frac{1}{2}}v^{-\frac{1}{2}}+B^{\frac{1}{2}}v^{-\frac{3}{2}}\right)e^{-Av-Bv^{-1}}dv=\frac{\sqrt{\pi}e^{-2\sqrt{AB}}}{2}\left(\mathrm{erf}\left(\sqrt{Ab}-\sqrt{Bb^{-1}}\right)-\mathrm{erf}\left(\sqrt{Aa}-\sqrt{Ba^{-1}}\right)\right).$$

In the second integral we substitute $\mu=A^{1/2}v^{1/2}+B^{1/2}v^{-1/2}$ and obtain

$$\frac{1}{2}\int_a^b\left(A^{\frac{1}{2}}v^{-\frac{1}{2}}-B^{\frac{1}{2}}v^{-\frac{3}{2}}\right)e^{-Av-Bv^{-1}}dv=\frac{\sqrt{\pi}e^{2\sqrt{AB}}}{2}\left(\mathrm{erf}\left(\sqrt{Ab}+\sqrt{Bb^{-1}}\right)-\mathrm{erf}\left(\sqrt{Aa}+\sqrt{Ba^{-1}}\right)\right).$$

Both integrals taken together are

$$\mathcal{I}_{-\frac{1}{2}}(a,b,A,B)=\frac{1}{2}\sqrt{\frac{\pi}{A}}\left(\mathcal{E}_{erf}\left(\sqrt{A},\sqrt{B},\sqrt{b}\right)-\mathcal{E}_{erf}\left(\sqrt{A},\sqrt{B},\sqrt{a}\right)\right). \qquad \text{(Equation 37)}$$

2. Next, we compute the integral $\mathcal{I}_{-\frac{3}{2}}(a,b,A,B)$. The variable substitution $v=u^{-1}$ transforms the integral $\mathcal{I}_{-\frac{3}{2}}$ to the integral $\mathcal{I}_{-\frac{1}{2}}$ we computed above

$$\mathcal{I}_{-\frac{3}{2}}(a,b,A,B) = \int_a^b v^{-\frac{3}{2}}e^{-Av-Bv^{-1}}dv=\mathcal{I}_{-\frac{1}{2}}\left(b^{-1},a^{-1},B,A\right).$$

We now use Equation 37 and obtain

$$\mathcal{I}_{-\frac{3}{2}}(a,b,A,B)=\frac{1}{2}\sqrt{\frac{\pi}{B}}\left(\mathcal{E}_{erf}\left(\sqrt{B},\sqrt{A},\sqrt{a^{-1}}\right)-\mathcal{E}_{erf}\left(\sqrt{B},\sqrt{A},\sqrt{b^{-1}}\right)\right).$$

For the solutions to Equations 1 and 3 we obtain

$$\mathcal{I}_{-\frac{3}{2}}(0,t,A,B)=\frac{1}{2}\sqrt{\frac{\pi}{B}}\mathcal{E}_{erfc}\left(\sqrt{B},\sqrt{A},\sqrt{t^{-1}}\right). \qquad \text{(Equation 38)}$$

3. Finally, we compute the integral $\mathcal{I}_{\frac{1}{2}}(a,b,A,B)$. This integral can be computed using integration by parts

$$\begin{aligned}\mathcal{I}_{\frac{1}{2}}(a,b,A,B) &= -\frac{1}{A}\left(v^{\frac{1}{2}}e^{-Av-Bv^{-1}}\right)\Big|_a^b + \frac{1}{2A}\int_a^b v^{-\frac{1}{2}}e^{-Av-Bv^{-1}}dv + \frac{B}{A}\int_a^b v^{-\frac{3}{2}}e^{-Av-Bv^{-1}}dv \\ &= -\frac{1}{A}\left(b^{\frac{1}{2}}e^{-Ab-Bb^{-1}} - a^{\frac{1}{2}}e^{-Aa-Ba^{-1}}\right) + \frac{1}{4A}\sqrt{\frac{\pi}{A}}\left(\mathcal{E}_{erf}\left(\sqrt{A},\sqrt{B},\sqrt{b}\right) - \mathcal{E}_{erf}\left(\sqrt{A},\sqrt{B},\sqrt{a}\right)\right) \\ &\quad + \frac{\sqrt{B\pi}}{2A}\left(\mathcal{E}_{erf}\left(\sqrt{B},\sqrt{A},\sqrt{a^{-1}}\right) - \mathcal{E}_{erf}\left(\sqrt{B},\sqrt{A},\sqrt{b^{-1}}\right)\right).\end{aligned}$$

Mathematical details on inverse Laplace transforms

Solving Equations 1 and 3 requires calculating the Laplace transform of $e^{-D\sqrt{s}}/(s-E)$. Here, we show that this Laplace transform is given by

$$\mathcal{L}^{-1}\left(\frac{e^{-D\sqrt{s}}}{s-E}\right) = \frac{1}{2}e^{Et}\mathcal{E}_{erfc}\left(\frac{D}{2},\sqrt{E},\sqrt{t^{-1}}\right). \qquad \text{(Equation 39)}$$

The function $e^{-D\sqrt{s}}/(s-E)$ can be represented as the product of two functions, whose inverse transformations are given by

$$\mathcal{L}^{-1}\left\{e^{-D\sqrt{s}}\right\} = \frac{De^{\frac{-D^2}{4t}}}{2\sqrt{\pi t^3}}, \quad \mathcal{L}^{-1}\left\{\frac{1}{s-E}\right\} = e^{Et}.$$

Since the inverse Laplace transformation of the product of two functions is the convolution of their inverse Laplace transformations we obtain

$$\mathcal{L}^{-1}\left(\frac{e^{-D\sqrt{s}}}{s-E}\right) = \frac{De^{Et}}{2\sqrt{\pi}}\int_0^t v^{-\frac{3}{2}}e^{-Ev-\frac{D^2}{4}v^{-1}}dv. \qquad \text{(Equation 40)}$$

By applying Equation 38 we obtain

$$\mathcal{L}^{-1}\left(\frac{e^{-D\sqrt{s}}}{s-E}\right) = \frac{De^{Et}}{2\sqrt{\pi}}\mathcal{I}_{-\frac{3}{2}}\left(0,t,E,\frac{D^2}{4}\right) = \frac{e^{Et}}{2}\mathcal{E}_{erfc}\left(\frac{D}{2},\sqrt{E},\sqrt{t^{-1}}\right). \qquad \text{(Equation 41)}$$

Solution of the diffusion equation

The diffusion equation

$$\frac{\partial F}{\partial t}(x,t) - \frac{\partial^2 F}{\partial x^2}(x,t) = f(x,t) \qquad \text{(Equation 42)}$$

with the initial condition $F(x,0)=0$ has the solution

$$F(y,t) = \int_0^t ds\int_{-\infty}^{\infty}\Phi(y-x,t-s)f(x,s)dx, \qquad \text{(Equation 43)}$$

where $\Phi(y,t) = e^{-y^2/(4t)}/(2\sqrt{\pi t})$. The function Φ is referred to as the fundamental solution of the Equation 42 with $f = 0$. We use this relation for the solution of Equation 22.